Black Holes through the lens of Matrix theory

Rishi Raj

A dissertation presented to the
Department of Physics at the
Indian Institute of Technology Madras
in partial fulfillment of requirements for the
Degree of Bachelor of Science (Hons)
and Master of Science

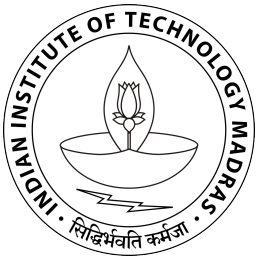

Supervisor: Dr. Ayan Mukhopadhyay
Co-supervisor: Dr. Vishnu Jejjala

May 2023

THESIS CERTIFICATE

This is to undertake that the thesis titled **Black Holes through the lens of Matrix theory**, submitted by me to the Indian Institute of Technology Madras, for the award of **Bachelor of Science (Hons) and Master of Science**, is a bona fide record of the research work done by me under the supervision of **Dr. Ayan Mukhopadhyay** and **Dr. Vishnu Jejjala**. The contents of this thesis, in full or in parts, have not been submitted to any other institute or university for the award of any degree or diploma.

Chennai 600036 **Rishi Raj**
Date: May 14, 2023

Dr. Ayan Mukhopadhyay
Research advisor
Assistant Professor
Department of Physics
IIT Madras

Dr. Vishnu Jejjala
Research co-advisor
Professor
School of Physics
University of the Witwatersrand

ABSTRACT

Holographic duality has been very successful at studying strongly-coupled gauge theories by mapping the problem to one of classical gravity. It is interesting to ask whether (and what) one can learn about quantum gravity by studying gauge theories in certain approximations.

In this dissertation, we present a summary of results in the study of the BFSS matrix model at high energies or, equivalently, weak coupling, where the dual gravity picture is highly stringy. The bosonic sector is analyzed through classical, real-time numerical simulations for a range of values of N (the size of matrices). We find sensitivity to initial conditions of a particular nature that suggests the following picture: typical (random) classical states of matrix theory mimic microstates of the dual gravitational theory.

Another feature reminiscent of black hole physics is random matrix behavior. The long-time distribution of matrices evolving through classical BFSS equations of motion is shown to resemble a traceless Gaussian Unitary Ensemble (GUE). We carefully match parameters on both sides (the matrix size N, the energy E of the state considered, and a scale parameter α of GUE). Lastly, we present evidence suggesting higher-order correlations than those arising from simple random matrix ensembles. We discuss possible causes and fixes.

PREFACE

I would like to express my sincere gratitude to my advisor and mentor, Dr. Ayan Mukhopadhyay[1] for the continuous support throughout my undergraduate study at IIT Madras. Since my first academic day, when I first met him, his encouragement and guidance and challenging me with hard physics problems have greatly impacted my current research abilities. He has constantly helped me with the writing of this thesis and the work it presents.

I would also like to thank my co-advisor, Dr. Vishnu Jejjala[2], for his invaluable insights during weekly discussions and his constant support during the writing of this thesis.

Besides the advisors for this thesis, I would like to thank Dr. Boris Pioline[3] for offering me the opportunity to work under his supervision in a summer internship in Paris on a related subject, Shivaprasad Hulyal (Engineering Physics major, IIT Madras) for his help with some of the simulations presented in this thesis, and Tanay Kibe (Doctoral Candidate, IIT Madras) for helpful discussions on the subject.

Lastly, this work would not have been successful without the constant and continuing support of my close friend, Ananya Shetty, and my parents, Ashok Kumar and Poonam.

[1]Associate Professor, Department of Physics, Indian Institute of Technology Madras

[2]Professor, School of Physics, University of the Witwatersrand

[3]Senior, Le Laboratoire de Physique Théorique et Hautes Énergies (LPTHE), Paris

CONTENTS

LIST OF FIGURES

LIST OF TABLES

CHAPTER

ONE

INTRODUCTION

General Relativity and the Standard Model of Particle Physics (a quantum field theory) have been incredibly successful at explaining physics at very long and short distance scales. However, it has been known for over a century that a fundamentally quantum mechanical description of gravity requires a drastic paradigm shift. The need for a theory of gravity is not just for aesthetics' sake but is fundamentally necessary to understand the physics of black holes and early cosmology.

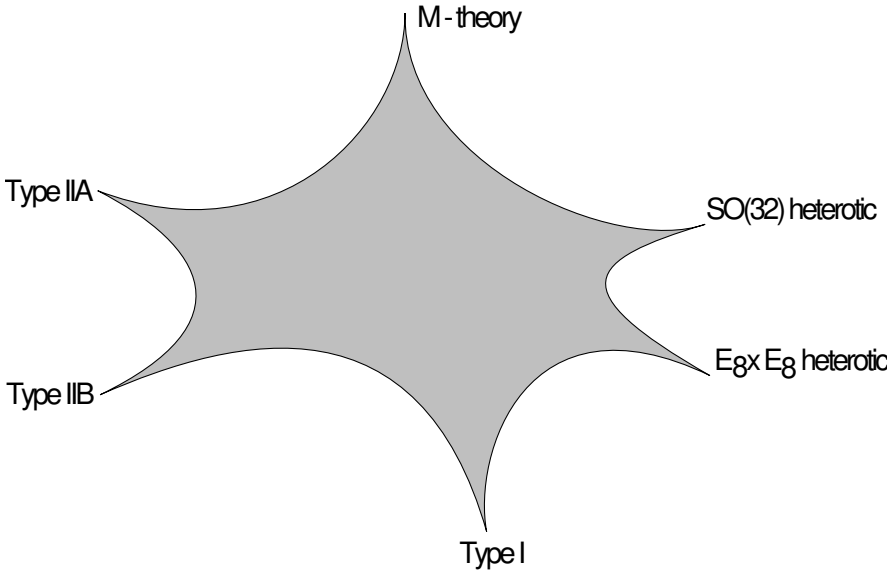

Figure 1.1: Various flavors of perturbative string theory as cusps of this diagram related by string dualities in appropriate limits (taken from [1])

It is common knowledge now that string theory provides a concrete realization of quantum gravity without any inconsistencies or divergences. String theory started its life as worldsheet perturbation theory. However, today, we understand that non-perturbative

aspects of string theory, particularly various dualities that relate seemingly different superstring theories, play a crucial role in the subject. The discovery of these dualities led to the famous picture of fig. 1.1 taken from [1]. Superstring theories should be thought of as asymptotic expansions around the cusps of this diagram. The description of physics in the "bulk" (finite distance away from the cusps) still eludes us.

One of the most outstanding consequences of string dualities is the gauge-gravity correspondence [2, 3]. The duality relates a gauge theory in d dimensional spacetime to quantum gravity (string theory) in $d+1$ dimensions, where the d dimensional spacetime is interpreted as the boundary of the $d+1$ dimensional bulk theory. It is a consequence of the open-closed string duality. See [4, 5] for excellent reviews of the conjecture. Many explicit examples of holographic correspondence have been found over the years, and the correspondence has been explicitly proved in certain situations [6, 7].

Gauge-gravity duality has been instrumental in understanding gauge theories and gravitational physics (i.e., black holes). It is an example of weak-strong duality, meaning that strongly coupled physics of gauge theories can be understood from weakly coupled gravity, where stringy corrections can be ignored. E.g., AdS/QCD is a theoretical framework that uses the gauge-gravity correspondence as a tool to study strongly coupled color physics of hadrons and baryons [8, 9]; AdS/CMT, a developing field, uses the duality to study complex condensed matter systems such as non-Fermi liquids and strongly correlated electrons and aspects of quantum criticality, and quantum entanglement in such systems [10, 11]. The utility of the duality goes both ways. Recently, it was used to compute the rate of Hawking evaporation of AdS black holes, the so-called Page curve [12, 13, 14]. A very accessible introduction to AdS/CFT is given in [15].

Matrix models are gauge theories in $0+1$ dimensions (i.e., quantum mechanics) that are amenable to a dual gravity description. The BFSS Matrix model was conjectured by T. Banks, W. Fischler, S. H. Shenker, and L. Susskind [16] to reproduce the S-matrix of 11-dimensional M-theory in certain limits. In particular, at low energies, M-theory reduces to the 11-dimensional Supergravity of E. Cremmer, B. Julia, and J. Scherk [17].

1.1 Motivation

One obtains two kinds of asymptotic expansions starting from Type IIA superstring theory. The string theory has two parameters, $\alpha' \propto \ell_s^2$ related to the string tension and length (ℓ_s), and the string coupling constant g_s that controls the contributions of world-sheets of various topologies. The string perturbation series at the lowest order in α' reproduces supergravity equations of motion. α' corrections represent stringy higher derivative corrections to the ordinary supergravity action. The 10-dimensional Plack length ℓ_p (or equivalently, Newton's constant G_N) is related to the string coupling g_s.

In a gauge theory, however, the important parameter is the 't Hooft coupling λ related to the Yang-Mills coupling $g_{\rm YM}$ as $\lambda = g_{\rm YM}^2 N$ where N is the rank of the gauge group $\mathrm{U}(N)$. In holographic duality, one can show that parameters on one side are related to

those on the other as follows

$$\frac{R^2_{\text{eff}}}{\alpha'} \sim \sqrt{\frac{\lambda}{r^3}} \tag{1.1}$$

$$g_s \sim \frac{\ell_p^4}{\ell_s^4} \sim \frac{\lambda}{N} \tag{1.2}$$

The first relation says that the effective radius of curvature measured in units of string length corresponds directly to the 't Hooft coupling (and the radial coordinate in the bulk r). Thus, in the regime where the radius of curvature is much larger than the string length (and we can trust ordinary supergravity without stringy corrections), the 't Hooft coupling is big, and the gauge theory is strongly coupled. Secondly, at fixed λ, taking a large N limit corresponds to taking $\ell_p \to 0$, in other words, ignoring quantum gravity corrections. This is precisely the regime where classical supergravity calculations hold!

Note that the 't Hooft coupling λ has dimensions of $(\text{energy})^3$; thus, low energies correspond to strong coupling and high energies to weak coupling. Further, due to eq. (1.1), the dual bulk geometry is highly curved near the boundary $r \to \infty$ and stringy corrections cannot be ignored. This is summarized in fig. 1.2 taken from [18].

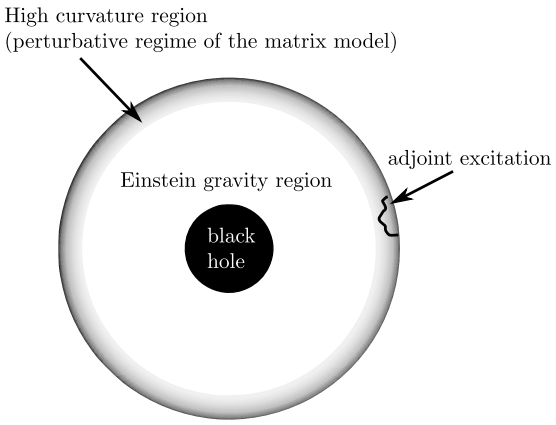

Figure 1.2: A schematic picture of the bulk geometry arising through the holographic correspondence. The boundary region is highly stringy, whereas classical gravity can be trusted in the deep bulk.

In this dissertation, we study the opposite limit, namely, the limit of large energies and hence of weak coupling in the matrix theory. This enables us also to take the classical limit and ignore quantum corrections to the leading order. Despite dropping quantum corrections, we find results reminiscent of black hole physics. Note that in this limit, the dual gravity picture is highly stringy, and in essence, we are attempting to explore near the boundary region of fig. 1.2.

1.2 Outline

In the next chapter, we will go through a quick review of the BFSS matrix model to set up notation and define the observables we study. In Chapter 3, we summarize our results: Section 3.2 demonstrates the precise nature of chaos in Matrix theory and the lessons to be learned from it. Section 3.3 highlights independence from initial conditions of the time statistics of various observables. Moreover, the last two sections talk about connections with random matrix theory. By comparing simulations with random matrix ensembles, we find that over long times and at large N, matrix model dynamics fit a random Gaussian Unitary ensemble (GUE) surprisingly well. We suggest and study various estimates for the parameters of this emergent random matrix ensemble. In the last section, we take note of the universal properties of matrix theory that depart from this random matrix behavior. The results presented in this chapter suggest the following picture of black hole microstates (see [19, 20]):

Random, time-dependent states (of D0-branes and strings stretching between them) in matrix theory mimic black hole microstates in the underlying quantum gravity.

The fuzzball program [21] is a similar attempt to parametrize the set of black hole microstates as fuzzball geometries which are highly stringy geometries without a horizon. The fuzzball proposal has lately been a subject of intense discussion and critique (see, e.g., [22]).

Finally, we end this dissertation by discussing our results, plans for the future, and open questions.

CHAPTER

TWO

LIGHTENING REVIEW

2.1 D0-brane Matrix Model

Many great reviews exist on the subject, e.g., [23, 24, 25]. The M-theory matrix model or the BFSS model can be obtained through three different methods (that are, in fact, equivalent)

a. Worldline theory of a large number (N) of D0 branes in type IIA string theory. [26]

b. Dimensional reduction of 9 + 1 dimensional Super Yang-Mills (SYM) theory to 0 + 1 dimensions [27].

c. Matrix regularization of the light-front quantized supermembrane theory [28].

The quantum mechanical model one obtains through this method has dynamical degrees of freedom that are $N \times N$ Hermitian matrices, and the structure of the theory is fixed entirely by three symmetries, SU(N), SO(9) and supersymmetry. In particular, one has 9 bosonic matrices (as in, adjoint of $\mathfrak{su}(N)$) X^i $i = 1, \ldots, 9$ that transform as an SO(9) vector and 16 fermionic matrices collectively called θ that transform as a Spin(9) Majorana spinor (each spinor component is an $N \times N$ matrix with grassmann odd elements).

The matrices X^i have the interpretation of the N D0-brane positions when they are simultaneously diagonal. The off-diagonal entries of X^i represent stringy degrees of freedom stretching from one D0-brane to another [29]. The complete action one obtains

through any of the above procedures (upto rescalings) is as follows

$$S[X,\theta,A] = \frac{1}{g_{\mathrm{YM}}^2}\int \mathrm{d}t\,\mathrm{Tr}\left(\frac{1}{2}D_tX^iD_tX^i + \frac{1}{4}\left[X^i,X^j\right]\left[X^i,X^j\right] + \frac{1}{2}\theta^T(iD_t\theta - \gamma_i\left[X^i,\theta\right])\right) \tag{2.1}$$

where the gauge covariant derivative acts as

$$D_tX^i = \dot{X}^i - i\left[A_t,X^i\right] \tag{2.2}$$

The parameter g_{YM}^2 is the Yang-Mills coupling and has dimensions of $(\text{energy})^3$. The relative coefficient between the bosonic and fermion parts of the action is fixed by supersymmetry. One can eliminate the $U(N)$ gauge field A by fixing the gauge $A_t = 0$. Further, we restrict our attention to states in the model with no fermionic modes $\theta = 0$. Thus, the reduced theory is a matrix model of 9 Hermitian matrices X^i with $i = 1,\ldots,0$ with the action

$$S[X] = \frac{1}{2g_{\mathrm{YM}}^2}\int \mathrm{d}t\,\mathrm{Tr}\left(\dot{X}^i\dot{X}^i + \frac{1}{2}\left[X^i,X^j\right]\left[X^i,X^j\right]\right) \tag{2.3}$$

The equations of motion are given by

$$\ddot{X}^i = -\left[\left[X^i,X^j\right],X^j\right] \tag{2.4}$$

The remnant of gauge fixing is the gauge constraint which follows from the A_t equation of motion before gauge fixing.

$$\left[\dot{X}^i,X^i\right] = 0 \tag{2.5}$$

A particularly nice way to visualize matrix configurations is to map them to embeddings of a sphere (or, more generally, of Riemann surfaces) in $\mathbb{R}^9$. This can be done for the sphere using matrix spherical harmonics (see appendix C). We have chosen to exclude any results or further discussion of matrix harmonics in this regard since this would require truncating the matrix model to two or three matrices and would distract us from the primary purpose of this thesis.

A curious consequence of the equations of motion eq. (2.4) is that configuration of matrices that are block diagonal, i.e.

$$X^i = \begin{pmatrix} A^i & \\ & B^i \end{pmatrix} \tag{2.6}$$

where A^i and B^i are submatrices, and the velocities $\dot{X}^i$ are also diagonal, then the equations of motion ensure that the block diagonal pieces evolve completely independently with no interactions. The interpretation is that separate clusters of D0-branes see no interactions in the classical matrix model. Indeed, a surprising and wonderful result of Matrix theory is that if one includes quantum corrections to the effective potential

between such clusters of D0-branes to one loop, we recover the classical supergravity interaction [30, 31, 32]. Indeed, this was pointed out by BFSS as a concrete test of their conjecture. In particular, in the simplest situation where two D0-brane particles are separated by a distance r and with a relative velocity v between them, the quantum effective potential around this background turns out to be

$$V = -\frac{15}{16}\frac{v^4}{r^7} + O\left(\frac{v^6}{r^{11}}\right) \tag{2.7}$$

to leading order in v/r^2. This is precisely the Newton-like classical potential that 11-dimensional supergravity between probe test particles reduces to in the quasi-static approximation (see [23] for an excellent review of matrix model interactions).

2.2 Scaling similarity

The gauge fixed BFSS action (including fermions) enjoys a scaling similarity under which

$$t \to \lambda^{-1} t \qquad X^i \to \lambda X^i \qquad \theta \to \lambda^{3/2}\theta \tag{2.8}$$

We call this transformation a similarity (and not a symmetry) because it does not keep the action invariant, but it changes by a factor

$$S[X, \theta] \to \lambda^3 S[X, \theta] \tag{2.9}$$

Hence, it is a symmetry of the equations of motion but not a symmetry of the full quantum theory. Since we will be doing classical simulations, we will exploit this similarity to normalize the energy surfaces we study to any positive energy, say, $E = 1$. We can always do this because the Hamiltonian

$$H = \frac{1}{2g_{\mathrm{YM}}^2}\,\mathrm{Tr}\left(\dot{X}^i\dot{X}^i - \frac{1}{2}\big[X^i, X^j\big]\big[X^i, X^j\big] + \theta^T\gamma_i\big[X^i, \theta\big]\right) \tag{2.10}$$

under eq. (2.8) scales like

$$H \to \lambda^4 H \tag{2.11}$$

Similarly, observables homogenous in the X^i such as $\mathrm{Tr}\, X^i X^i$ scale in a specific way under eq. (2.8). e.g.

$$\mathrm{Tr}\, X^i X^i \to \lambda^2\, \mathrm{Tr}\, X^i X^i \tag{2.12}$$

Thus, we restrict attention to observables of this type. Further, we rescale all our variables so that $g_{\mathrm{YM}} = 1$.

2.3 Recent results

Many efforts have been made to understand non-perturbative aspects of string/M-theory via dual Matrix models using numerical methods. These primarily focus on Monte

Carlo-type simulations in Euclidean spacetime (see [33, 34] for a review). What distinguishes our work from the papers just cited is that we are working in a regime of Matrix theory where there are enormous stringy corrections in the dual quantum gravity. Thus, no simple description or expectations exist on that side. Further, we do real-time classical simulations instead of periodic Euclidean time path integrals. Despite this, we find behavior reminiscent of ordinary black holes, such as random matrices and the typicality of microstates.

The Monte Carlo methods used in [33] have been quite successful at doing precision tests of the holographic correspondence. For instance, the thermodynamic relations for the dual black geometry (see [18]) have been derived numerically for large matrices where the result holds, including higher derivative corrections [35]. Further, an interesting observable in these gauge theories that we will not have much to say about (since we are not working in Euclidean time) is the Polyakov loop in an $\mathfrak{su}(N)$ representation R

$$W_R = \mathrm{Tr}_R \, \mathcal{P} \exp\left(i \oint A \right) \tag{2.13}$$

where the integral is taken over periodic Euclidean time. The thermal expectation value of this operator is an order parameter for confinement in pure gauge theories. In [36], confinement in strong coupling limit of gauge theories was studied using dual gravity. Monte Carlo techniques have recently been used to confirm this M-theory picture [37].

CHAPTER

THREE

SUMMARY OF NUMERICAL STUDIES

Having defined the classical system we wish to study, we use standard numerical practices to obtain the time evolution of Matrix theory observables. The details of the numerical methods can be found in appendix A.

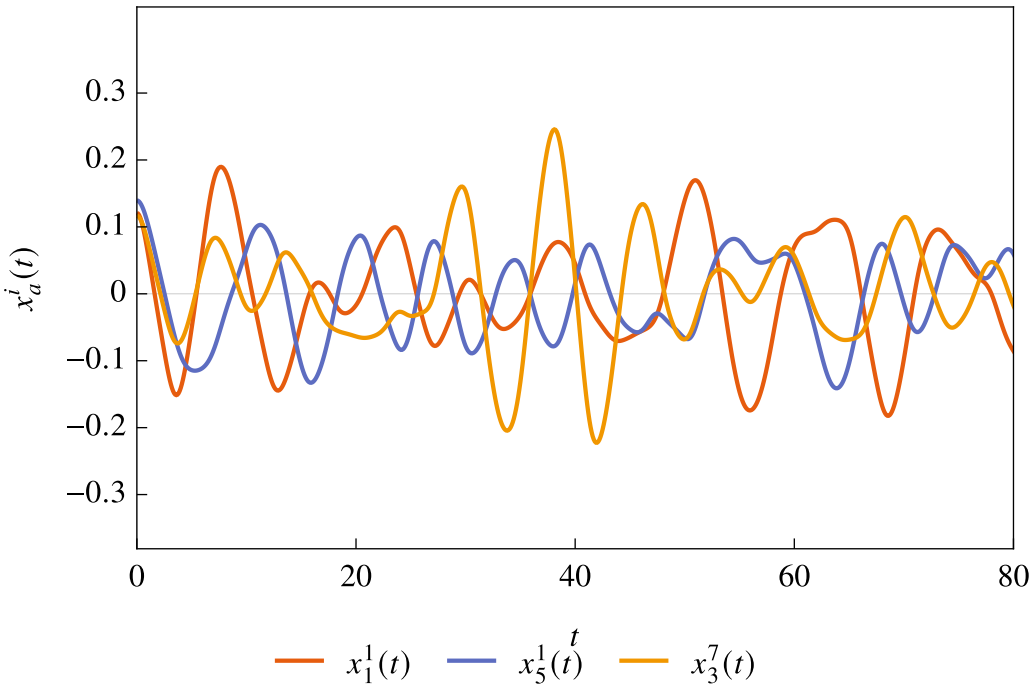

Figure 3.1: Numerical simulation of a few matrix coefficients starting with random initial conditions of the kind described in appendix A for $N = 9$

We restrict our attention to initial conditions of a specific type. Namely, those with zero initial velocities

$$\dot{X}^i(0) = 0 \tag{3.1}$$

This has two benefits:

a. The Gauss constraint
$$\left[X^i, \dot{X}^i\right] = 0 \tag{3.2}$$
is automatically satisfied at $t = 0$. Moreover, since the constraint is a constant of motion (as always with gauge constraints), time evolution (if done correctly) guarantees that the constraint will always be satisfied.

b. The SO(9) angular momentum
$$\mathcal{J}^{ij} = \mathrm{Tr}\left(X^i \dot{X}^j - X^j \dot{X}^i\right) \tag{3.3}$$
which is also a conserved charge, vanishes at all times. In other words, we are looking at the zero angular momentum sector of BFSS, and there are good reasons to do so [38].

The initial "positions" $X^i(0)$ are taken to be random Hermitian matrices (see appendix A), and we study many such random states for different sizes of matrices N. The time evolution of a typical such state (or rather, of its coefficients in an $\mathfrak{su}(N)$ basis) looks as in fig. 3.1

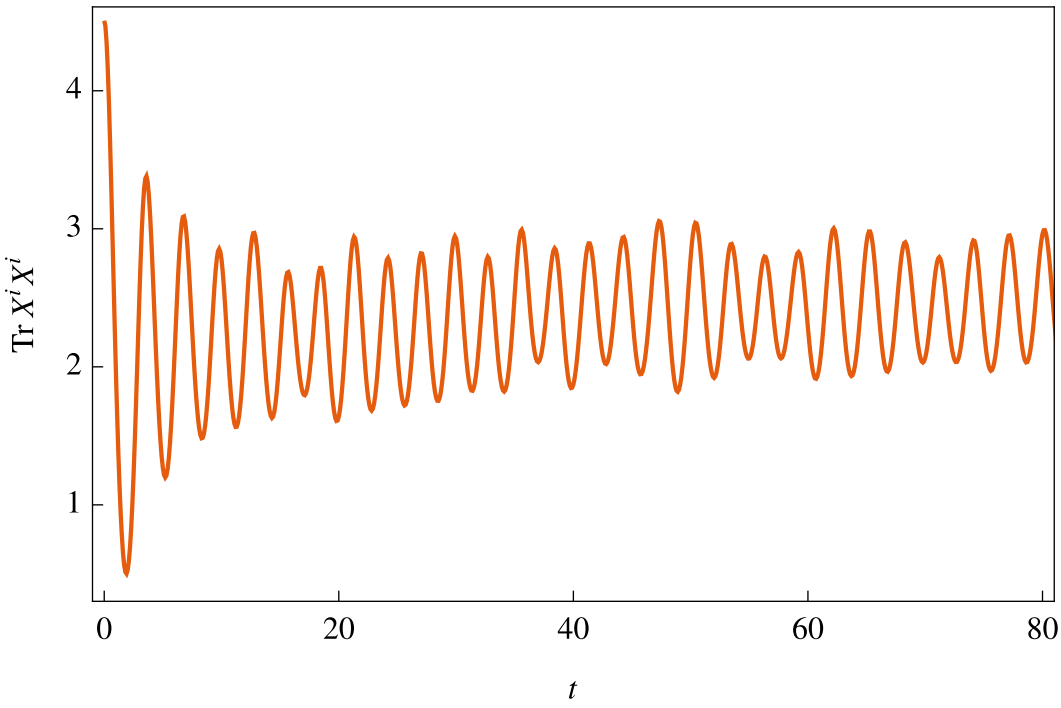

Figure 3.2: Dynamics of the simplest gauge and rotational invariant operator $\mathrm{Tr}\, X^i X^i$ for the state in fig. 3.1

3.1 Horizon Dynamics

When the BFSS Matrix model has a tractable classical supergravity dual, the black brane solution has a horizon whose radius r_0 can be related to the observable $\mathrm{Tr}\, X^i X^i$ in the

matrix model.

$$r_0 \sim \sqrt{\frac{1}{N}\operatorname{Tr} X^i X^i} \tag{3.4}$$

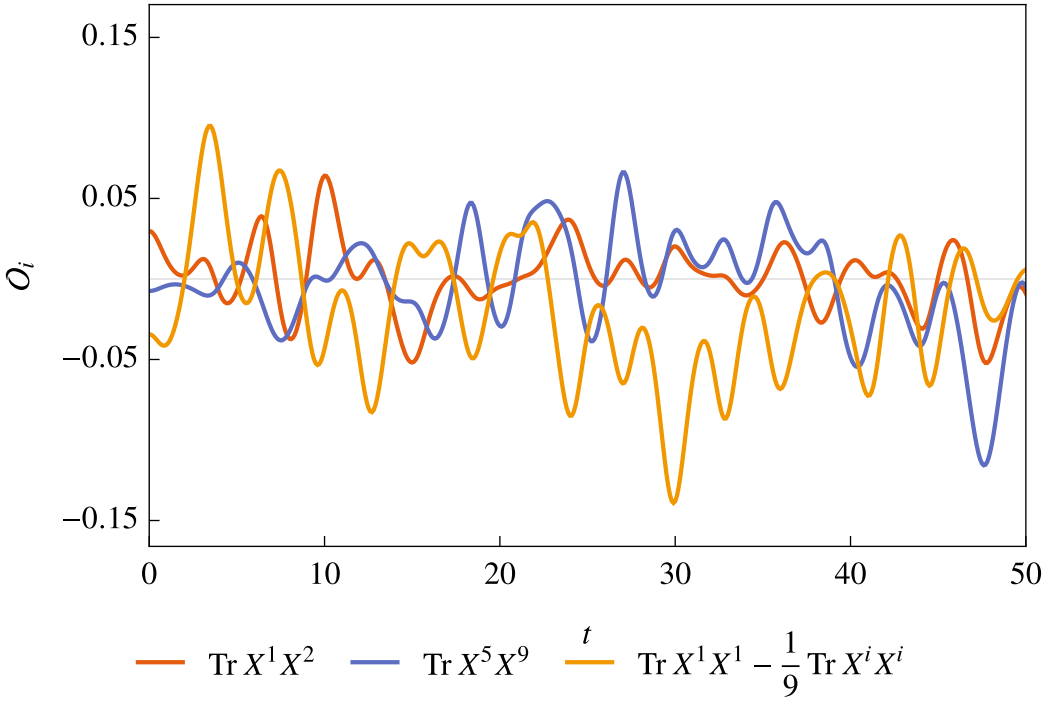

Figure 3.3: Few components of the symmetric traceless tensor $\mathfrak{S}^{ij}$ for the state in fig. 3.1

Therefore, one expects that the time evolution of $\operatorname{Tr} X^i X^i$ captures the microscopic dynamics of the black hole horizon in the underlying geometry. For the state in fig. 3.1, the corresponding dynamics of $\operatorname{Tr} X^i X^i$ is shown in fig. 3.2

Other interesting observables can be constructed from single trace higher order polynomials in the Xs. In supergravity, these can be interpreted as higher order multipoles, deviations from SO(9) spherical invariance. The simplest one is the symmetric traceless SO(9) tensor

$$\mathfrak{S}^{ij} = \operatorname{Tr}\left(X^i X^j\right) - \frac{\delta^{ij}}{K}\operatorname{Tr}\left(X^k X^k\right) \tag{3.5}$$

along with other higher-order observables, such as

$$\mathfrak{C}^{i}_{(3a)} = \operatorname{Tr}\left(X^i X^j X^j\right) \tag{3.6}$$

$$\mathfrak{C}^{ijk}_{(3b)} = \operatorname{Tr}\left(X^{(i} X^j X^{k)}\right) \tag{3.7}$$

$$\mathfrak{Q}_{(4a)} = \operatorname{Tr}\left(X^i X^j X^i X^j\right) \tag{3.8}$$

$$\mathfrak{Q}_{(4b)} = \operatorname{Tr}\left(X^i X^j X^j X^i\right) \tag{3.9}$$

A few components of $\mathfrak{S}^{ij}$ and $\mathfrak{Q}_{(4a)}$ are shown for the state in fig. 3.1 in fig. 3.3, and fig. 3.4

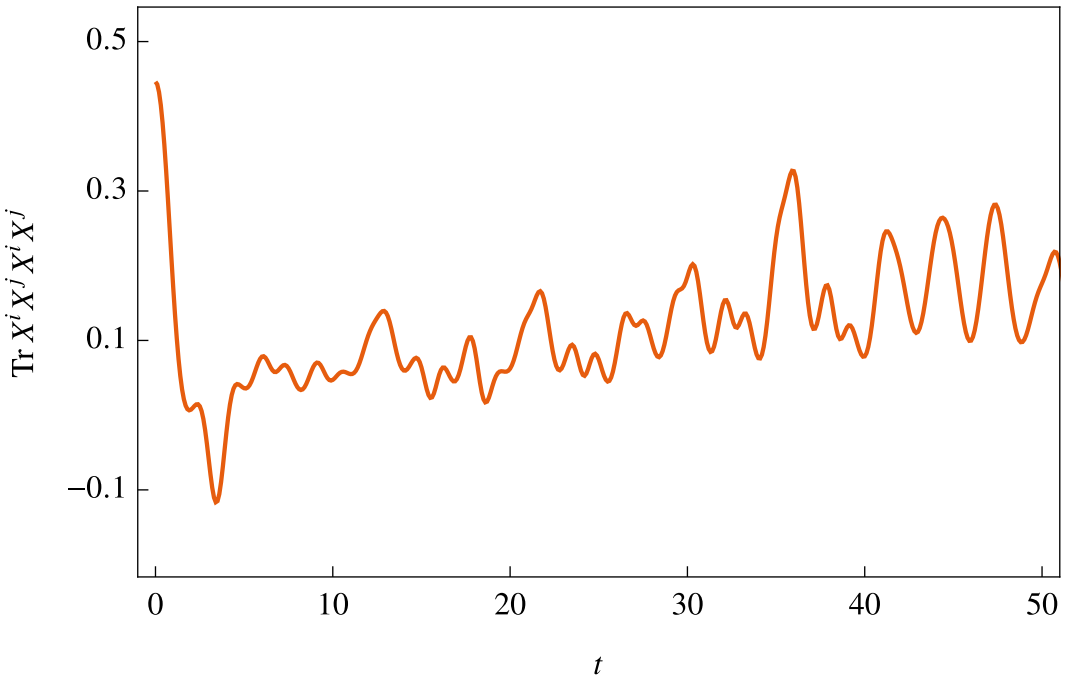

Figure 3.4: One of the two quartic observables $\mathfrak{Q}_{(4a)}$. Note that it forms one-half of the bosonic potential of BFSS

3.2 Sensitivity to initial conditions

The bosonic model under consideration exhibits sensitivity to initial conditions. One can see this explicitly by considering two random initial states that differ by a small amount ϵ. To achieve this, generate two initial conditions $X_{(\text{orig})}$ and $X_{(2)}$ in the manner demonstrated in appendix A and define

$$X_{(\text{pert})} = X_{(\text{orig})} + \epsilon X_{(2)} \tag{3.10}$$

where the matrix and SO(9) vector indices have been supressed. The result of numerically evolving these states for $\epsilon = 10^{-6}$ is given in fig. 3.5. Not that the two trajectories for the matrix elements and the gauge invariant observable $\text{Tr}\, X^i X^i$ diverge at slightly different times.

One can quantify this dependence on initial conditions by considering an appropriate gauge invariant distance between the two states. One way is to define it as

$$R^2 = \sum_i \text{Tr}\left(X^i_{(\text{pert})} - X^i_{(\text{orig})}\right)^2 \tag{3.11}$$

One can go even further and do this for an entire cloud of initial conditions. Suppose we start with m initial conditions $X_{(a)}$ $(a = 1, \ldots, m)$ that are ϵ away from each other in the manner described above. The average location of these states is

$$Z^i = \frac{1}{m} \sum_a X^i_{(a)} \tag{3.12}$$

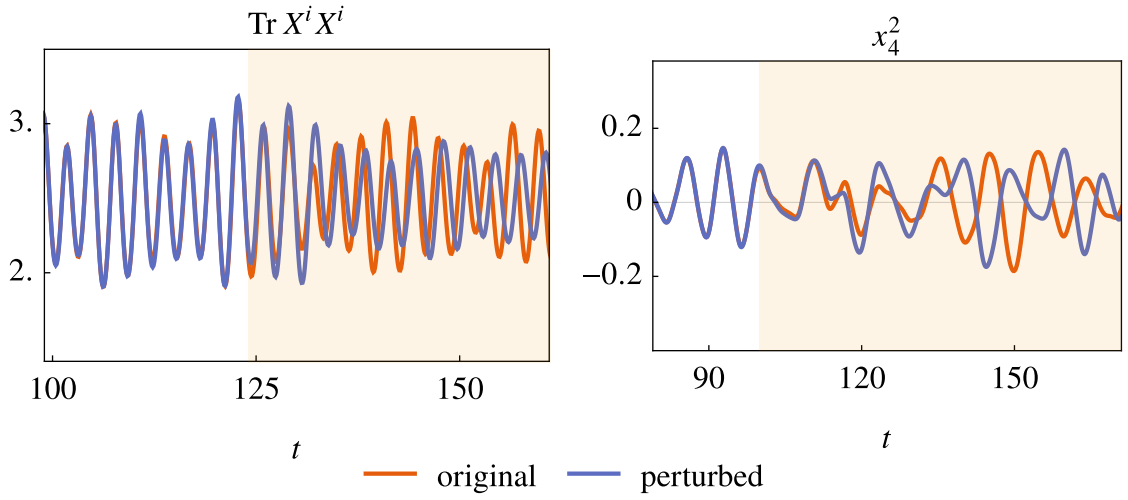

Figure 3.5: A demonstration of chaos in the classical dynamics. Both plots show the dynamics of two states that start very close to each other $\epsilon \sim 10^{-6}$ but eventually diverge.

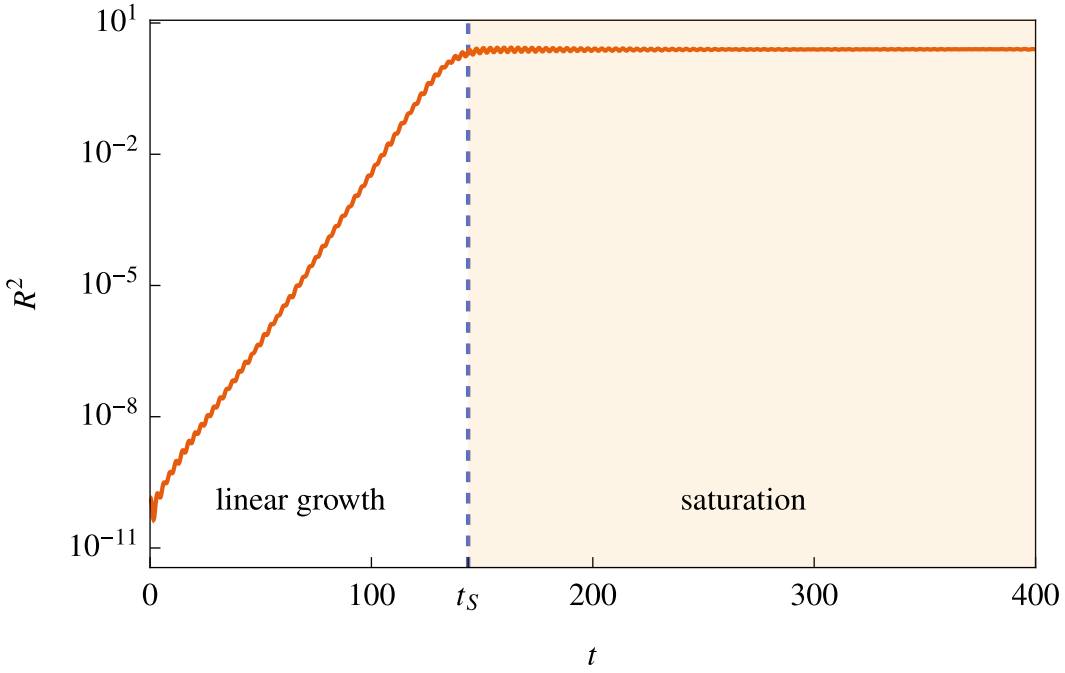

Figure 3.6: A log-scale plot of the spread of states in phase space R^2 as a function of time. Note the two phases: linear growth followed by saturation

A straightforward generalization of eq. (3.11) is

$$R^2 = \frac{1}{m} \sum_{a,i} \mathrm{Tr} \left(X^i_{(a)} - Z^i \right)^2 \tag{3.13}$$

A plot of R^2 starting at $m = 48$ initial conditions close to each other within $\epsilon = 10^{-6}$ is shown in fig. 3.6. Remarkably, one observes two well-separated regions of time, best seen on a log scale. The distance measure starts growing linearly, as expected in a typical chaotic system. It does this until a time t_S, around which it settles down into an almost

constant value. This saturation region extends to arbitrarily long times, and we shall call t_S the *saturation time*.

This feature of an initial regime of linear growth followed by saturation is observed universally at all points on the phase space and for all values of the parameters under consideration: matrix size N, number of matrices K, and the number of initial conditions m.

One way to visualize this is to take three-dimensional sections of the entire phase space and observe the trajectories of the various states. One finds precisely as one expects: the trajectories start in a tiny dense ball (of size $\sim \epsilon$) and initially evolve as a single state at the location of the ball would. However, the ball grows as it evolves until it gets big enough to fill a sizable portion of phase space. Around $t = t_S$, the ball stops growing, but the various points that make up this gas of states start jiggling around endlessly while maintaining its approximate shape and size.

So far, we have discovered a dynamical time scale: the saturation time t_S. Later when we look at statistics of various observables over long times, it would be helpful to exclude the initial region of linear growth and compute statistics from, say, $t = 200 > t_S$ to $t = T$ where we take T to be of the order of 1000 or 10,000.

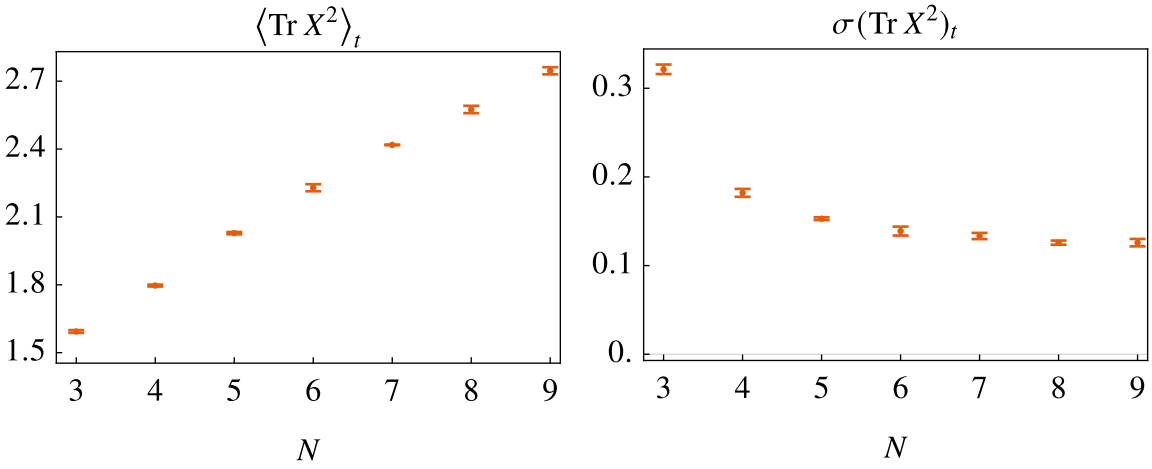

Figure 3.7: The time average (left) and standard deviation (right) of $\mathrm{Tr}\, X^2$ for many states of normalized energy $E = 1$ as a function of matrix size N. The error bars indicate the dependence of the statistic on the chosen initial condition.

3.3 Memorylessness

Upon looking at fig. 3.6, it is very tempting to suggest that even though the precise dynamical evolution of states is highly initial condition dependent, the overall features, such as long-time averages of various observables might lose such dependence on the initial state. If this is the case, due to the scaling similarity of eq. (2.8), one would expect long time averages of observables homogenous in the Xs to only depend on the energy of the energy surface being explored. This dependence follows easily from the scaling relations eq. (2.8).

The most straightforward check for solution independence is to compute the long-time averages (and higher statistics) of various observables. This is done in fig. 3.7 for $\mathrm{Tr}\, X^i X^i$ and in fig. 3.8 for the symmetric traceless tensor $\mathfrak{S}^{ij}$ of eq. (3.5) for different matrix sizes. The error bars in the figures indicate how much the corresponding statistic changes for different initial conditions of the same energy.

From these figures, it seems that certain observables like $\mathrm{Tr}\, X^i X^i$ exhibit universal behavior at long times more than others, even though the trend indicates that perhaps more and more higher-order observables start to "thermalize" (obtain stable time averages) as we go to larger values of N.

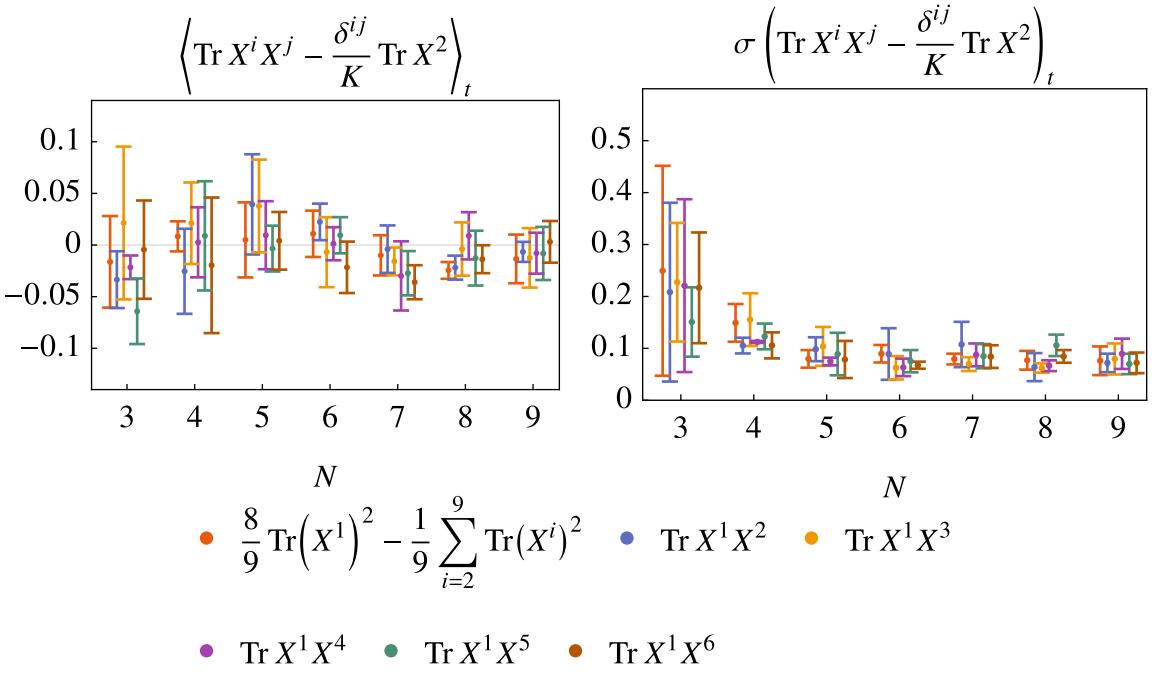

Figure 3.8: Time statistics for a few components of the symmetric traceless tensor $\mathfrak{S}^{ij}$.

Random matrix theory suggests that a critical observable in any matrix model is the set of eigenvalues of the matrices. In fig. 3.9, we plot the (time) distribution of the eigenvalues of the various X^i. We do not specify which X^i because these distributions look more or less exactly the same (up to numerical inaccuracies) for different matrices X^i. The plots show this distribution arising from two different initial conditions, (a) and (b). The almost perfect overlap between them is more evidence to support memorylessness.

For those familiar with random matrix distributions, fig. 3.9 would appear a familiar pattern. Indeed, this is qualitatively, the shape of the distribution of eigenvalues for a Gaussian Unitary Ensemble (GUE). This observation will be explored further in the next section.

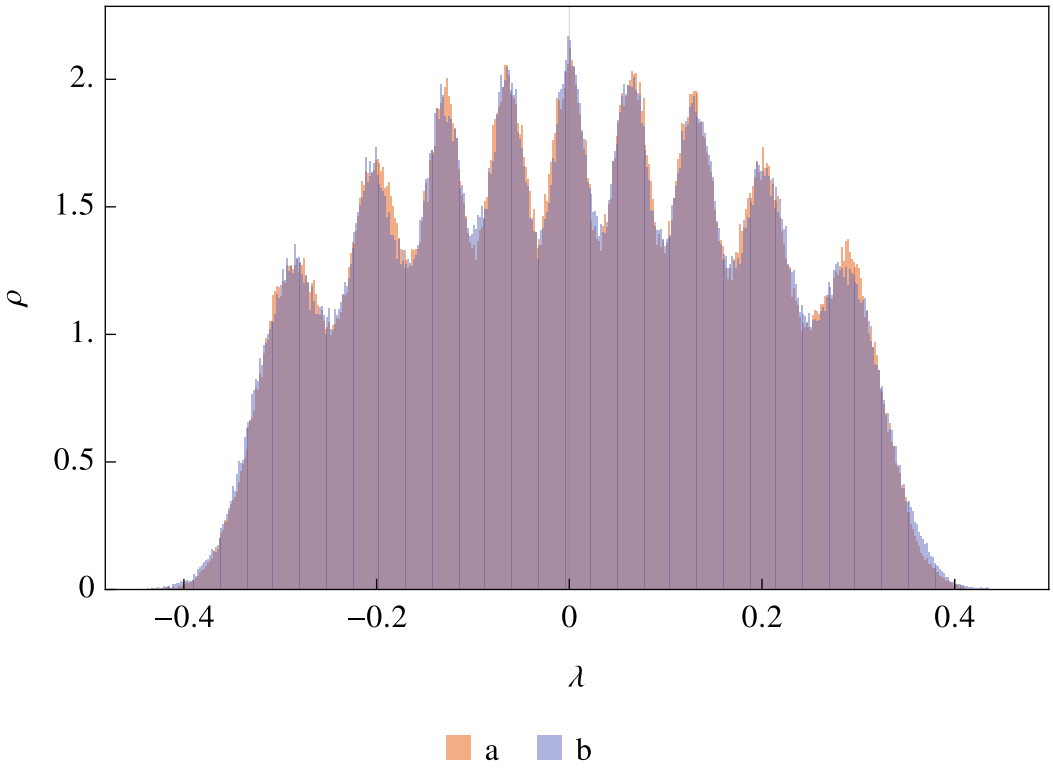

Figure 3.9: The eigenvalue (time) distribution for $N = 9$ starting at two random initial states (a) and (b). Note that all eigenvalues (of all matrices X^i) have been clubbed together since they have identical distributions.

Lastly, one can also look at the full distribution of $\mathrm{Tr}\, X^i X^i$. This is shown in fig. 3.10. The overlap, in this case, is not as good as the eigenvalues but is satisfactory enough to take memorlylessness as a feature of the bosonic model we are studying seriously.

3.4 Connections to random matrices

We will not explore in greater detail the observation that the eigenvalue distribution arising from the time evolution of the matrix eigenvalues looks suspiciously close to a Gaussian random matrix distribution of Hermitian matrices.

Perhaps the most preliminary question in this regard is the covariance matrix $\mathrm{Cov}(X^i, X^j)$ or equivalently, in a suitable $\mathfrak{su}(N)$ basis, the object

$$c_{ia,jb} = \mathrm{Cov}\left(x^i_a, x^j_b\right) \tag{3.14}$$

Since each matrix has N^2-1 components and there are K of them, this is a $(K(N^2-1))\times(K(N^2-1))$ real symmetric matrix. For $K = 9, N = 9$, $K(N^2-1) = 720$. Evaluating this matrix is a straightforward task. We observe that this matrix is almost diagonal.

Very qualitatively, it looks like

$$\lambda^2 \begin{pmatrix} 1 \pm \epsilon & \pm\epsilon & \dots \\ \pm\epsilon & 1 \pm \epsilon & \dots \\ \vdots & \vdots & \ddots \end{pmatrix} \tag{3.15}$$

with $\epsilon \approx 5\%$. Here, λ sets the scale of the x_a^is and is an important quantity we will return to. Another way to demonstrate this is through fig. 3.11, which shows the distribution of the diagonal and off-diagonal elements of the covariance matrix one obtains. As claimed, the matrix coefficients x_a^i are distributed in an almost i.i.d. way, at least up to second-order correlations.

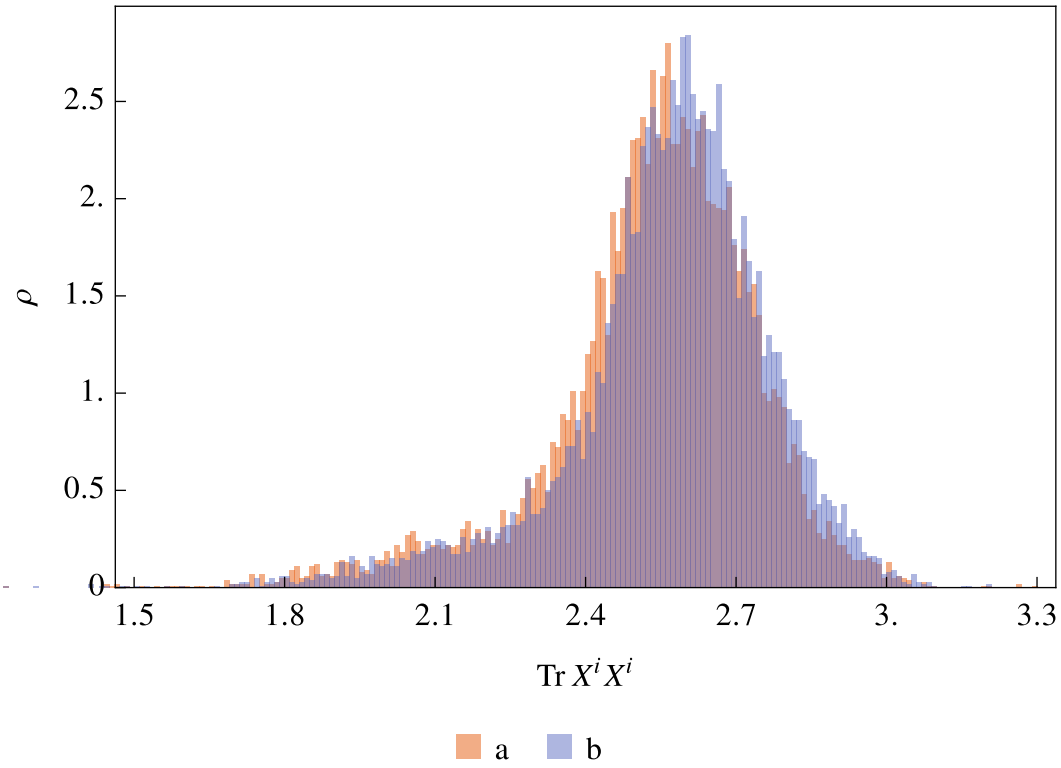

Figure 3.10: The (time) distribution of $\operatorname{Tr} X^i X^i$ for the same two random states in fig. 3.9. Note that the purplish color indicates the region where the distributions overlap.

If one had to guess a form for the distribution of the x_a^is based on the covariance matrix and on the observation that higher central moments tend to be quite small, the most natural choice would be a multivariable gaussian

$$p(x) \sim \exp\left(-\mu \sum_{ia} x_a^i x_a^i\right) \tag{3.16}$$

However, based on our conventions for the $\mathfrak{su}(N)$ basis (appendix A), the quantity inside the exponential is just $\operatorname{Tr} X^i X^i$ up to a numerical factor.

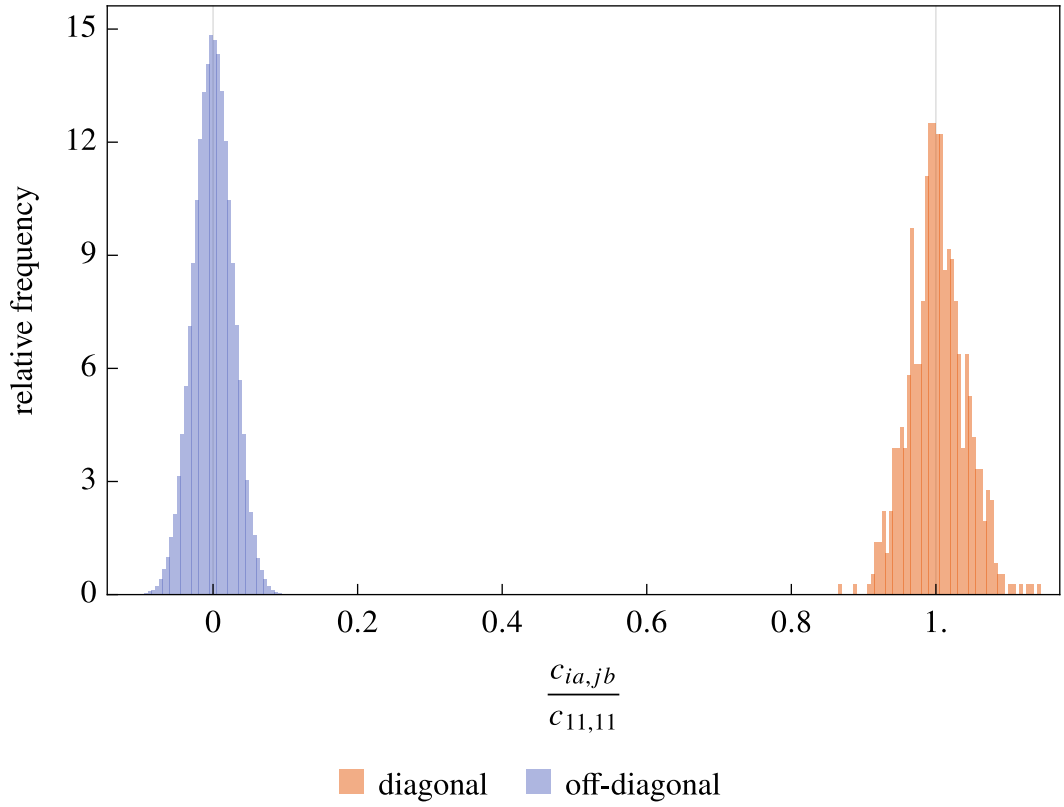

Figure 3.11: distribution of the covariance matrix elements (normalized by one of the diagonal values). Note how the spread is around $\epsilon \sim 5\%$.

Thus, we make the conjecture that the matrices X^i look as if they are identically and independently distributed from a traceless Gaussian Unitary Ensemble (GUE) (see appendix B) of rank N. In other words, the distribution $p(X)$ of the matrices over long times (and for large N, as we will see) is

$$p(X) = \left(\frac{\alpha^{(N^2-1)/2}}{Z_{\text{tGUE}}}\right)^K \exp\left(-\frac{\alpha N}{2}\sum_i \text{Tr}\, X^i X^i\right) \tag{3.17}$$

where Z_{tGUE} is the partition function of traceless GUE, for normalization, and α sets the scale of X^is. Due to (a) the solution independence of various distributions we looked at and (b) the scaling similarity eq. (2.8), it is reasonable to expect that the scale parameter α depends only on N and the scale λ, or equivalently, the energy E of the solution as follows

$$\alpha = \alpha(N, E) = \frac{\alpha_N}{\sqrt{E}} \tag{3.18}$$

We can explicitly verify this claim by finding an estimate for α from the simulations and then comparing the random matrix ensemble at this estimated value for α and the simulations themselves. Note that all our simulations have normalized energy $E = 1$, so we need not worry about the dependence of α on E: we are directly estimating α_N. We consider the following estimates

a. For physical reasons, our primary estimate would come from the distribution of $\text{Tr}\, X^i X^i$ itself. In particular, both the mean and the variance of this distribution are

meaningful quantities to compare to. In essence, we are using a method of moments estimate for the population parameter α. It is quite straightforward to show that $\operatorname{Tr} X^i X^i$ follows a gamma distribution (essentially a scaled χ^2-distribution)

$$\operatorname{Tr} X^i X^i \sim \Gamma\left(\frac{K(N^2-1)}{2}, \frac{2}{\alpha N}\right) \tag{3.19}$$

Thus the mean (μ) and variance (σ^2) of $\operatorname{Tr} X^i X^i$ are

$$\mu = \frac{K(N^2-1)}{\alpha N} \tag{3.20}$$

$$\sigma^2 = \frac{2K(N^2-1)}{\alpha^2 N^2} \tag{3.21}$$

Or, for the estimate $\hat{\alpha}_N$, we have (using just the mean μ)

$$\hat{\alpha}_N = \frac{K(N^2-1)}{N \langle \operatorname{Tr} X^i X^i \rangle} \tag{3.22}$$

b. The matrix coefficients x_a^i follow a Gaussian distribution. Indeed, this was the first step towards the conjecture. The means, in this case, are not very meaningful since, on both sides, these are very close to zero. However, the variance (σ^2) can be used to estimate α since

$$\sigma^2 = \frac{2}{\alpha N} \tag{3.23}$$

from eq. (3.17). Or, for the estimate

$$\hat{\alpha}_N = \frac{2}{N \operatorname{Var}\left(x_a^i\right)} \tag{3.24}$$

c. An object simpler than $\operatorname{Tr} X^i X^i$ but is not SO(9) invariant is $\operatorname{Tr}\left(X^1\right)^2$. It is distributed according to

$$\operatorname{Tr}\left(X^1\right)^2 \sim \Gamma\left(\frac{N^2-1}{2}, \frac{2}{\alpha N}\right) \tag{3.25}$$

and so, we have two estimates

$$\hat{\alpha}_N = \frac{N^2-1}{N \left\langle \operatorname{Tr}\left(X^1\right)^2 \right\rangle} \tag{3.26}$$

from the mean and

$$\hat{\alpha}_N = \frac{\sqrt{2(N^2-1)}}{N \operatorname{SD}\left(\operatorname{Tr}\left(X^1\right)^2\right)} \tag{3.27}$$

from the standard deviation.

d. A component of the symmetric traceless tensor $\mathfrak{S}$, e.g. $\mathfrak{S}^{12} = \operatorname{Tr} X^1 X^2$. The distribution of this object is some generalized gamma distribution. However, to save time, an easier way to estimate α is to numerically generate a large sample of matrices Y^i according to eq. (3.17) with $\alpha = 1$, compute the observable in question:

in this case, $\mathrm{Tr}\, Y^1 Y^2$ and compare ratios of the statistics (e.g., the variance, since the mean is practically zero). The estimate we use here is

$$\hat{\alpha}_N = \frac{\mathrm{SD}\left(\mathrm{Tr}\, Y^1 Y^2\right)}{\mathrm{SD}\left(\mathrm{Tr}\, X^1 X^2\right)} \tag{3.28}$$

e. The combined eigenvalue distribution: We do not have a closed-form expression for this distribution. It is likely some combination of Hermite polynomials (appendix B). But the simpler thing is to generate a large sample Y^i with $\alpha = 1$, compute the eigenvalues λ_Y and use

$$\hat{\alpha}_N = \frac{\mathrm{Var}\left(\lambda_Y\right)}{\mathrm{Var}\left(\lambda_X\right)} \tag{3.29}$$

The result of doing this exercise is summarized in table 3.1 below. As stated earlier, the primary estimate for α_N comes from the mean of the distribution of $\mathrm{Tr}\, X^i X^i$. These values of α_N for $N = 3, \ldots, 9$ are shown in fig. 3.12 with error bars indicating the dependence on initial conditions. It is interesting to ask whether this N-dependence can be obtained from some fundamental considerations about the matrix model and supergravity. At present, we do not have an answer to this. However, the N dependence (for large N) can be worked out numerically and turns out to be approximately

$$\alpha_N \approx 2.21 N^{0.529} \tag{3.30}$$

One can see this on a log-log plot of the α_N estimates and the function eq. (3.30). This is shown in fig. 3.13.

N	$\left\langle \mathrm{Tr}\, X^i X^i \right\rangle$	$\sigma\left(x_a^i\right)$	$\left\langle \mathrm{Tr}\left(X^1\right)^2 \right\rangle$	$\sigma(\mathrm{Tr}\left(X^1\right)^2)$	$\sigma\left(\mathrm{Tr}\, X^1 X^2\right)$	$\sigma\left(\lambda\right)$
3	15.06(6)	14.89(21)	14.6(25)	12.6(21)	11.5(22)	14.85(21)
4	18.78(5)	18.91(38)	18.5(12)	16.1(12)	16.1(16)	18.93(38)
5	21.30(6)	22.10(26)	22.36(59)	20.7(11)	19.9(12)	22.09(26)
6	23.55(17)	24.53(23)	24.66(51)	22.5(9)	22.7(12)	24.52(23)
7	25.52(2)	27.14(13)	27.39(42)	24.6(16)	25.7(14)	27.16(13)
8	27.53(18)	29.28(16)	29.12(33)	25.6(13)	27.9(14)	29.28(16)
9	29.13(17)	31.22(21)	31.17(40)	27.6(10)	28.9(15)	31.22(21)

Table 3.1: Estimates for α_N. The header indicates which statistic was used for the estimate. The statistics used for this table were taken from $\sim$ 30 initial conditions for $T = 1000$ with step size $dt = 0.1$

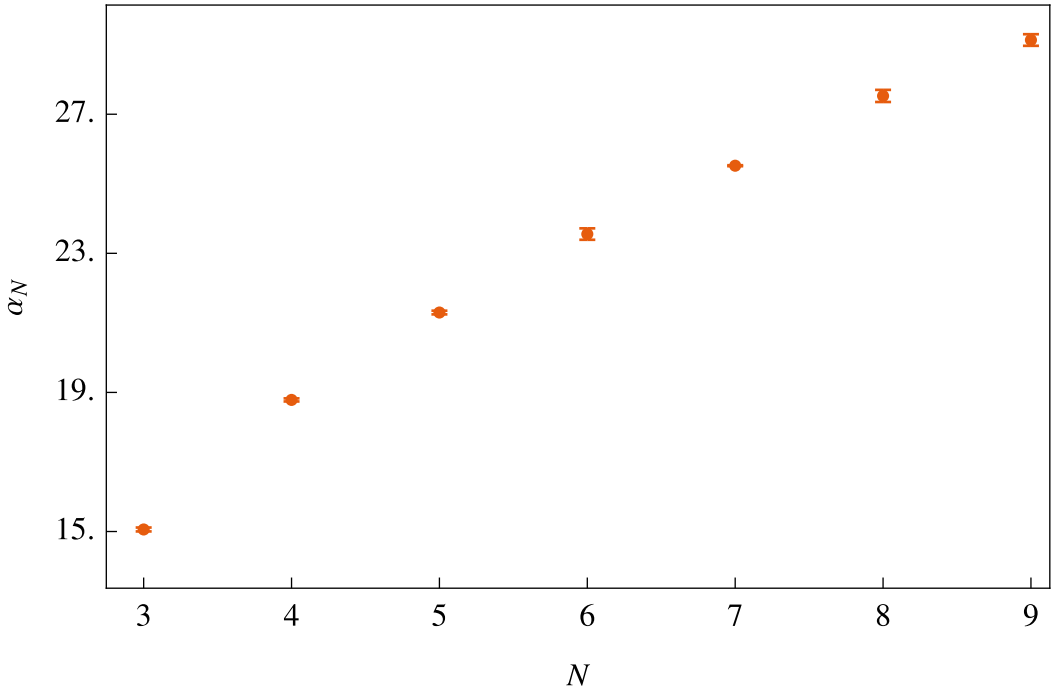

Figure 3.12: Primary estimate for α_N (computed using $\langle \mathrm{Tr}\, X^i X^i \rangle$) as a function of N. Again, error bars indicate variation across initial conditions.

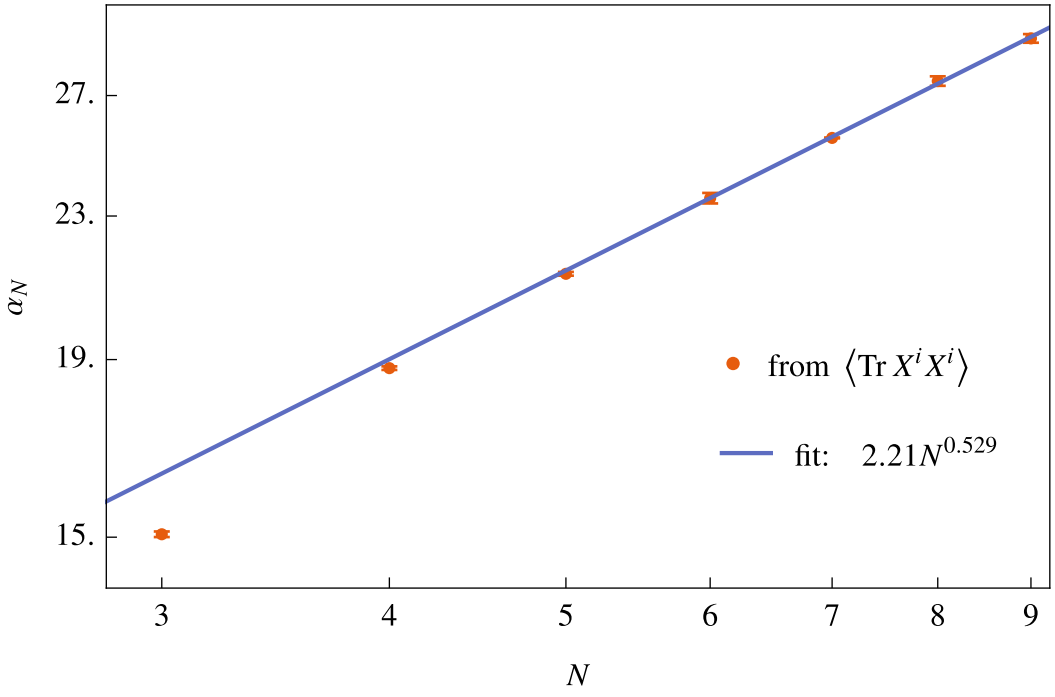

Figure 3.13: estimate for α_N (fig. 3.12) in a log-log scale along with a linear fit for the last few points.

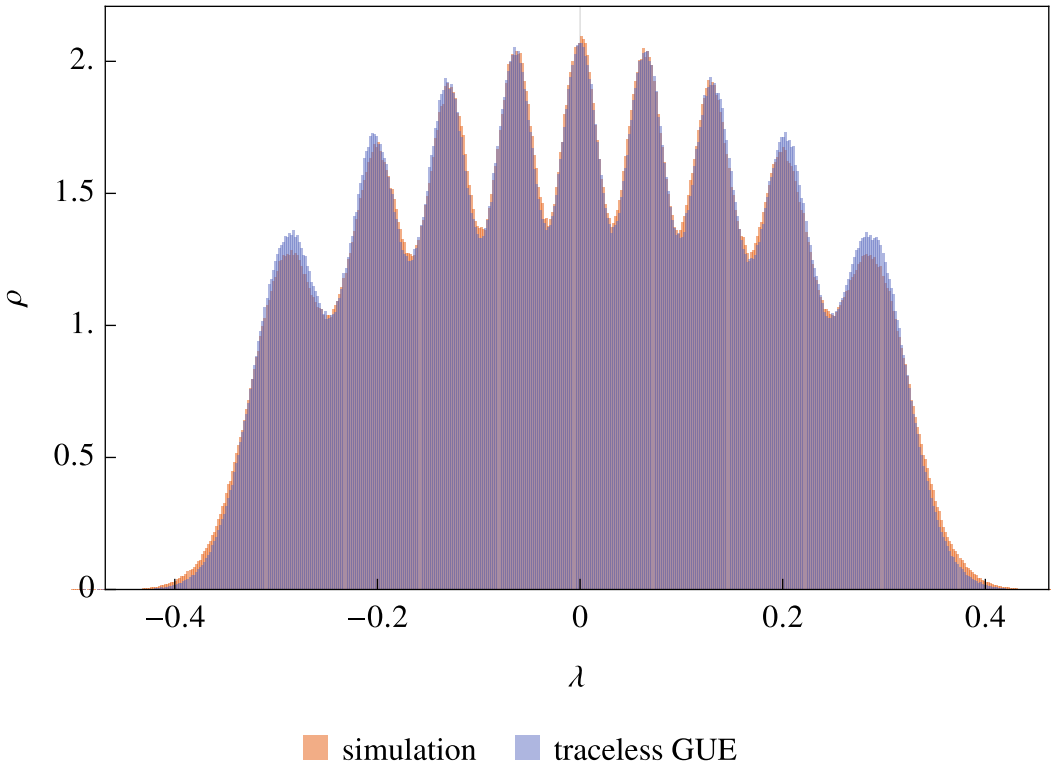

Figure 3.14: Eigenvalue distribution at $N = 9$ for matrices obtained through a simulation and the corresponding distribution from traceless GUE, eq. (3.17) with α given in table 3.1.

Having fixed a value of α, one can finally ask whether the simulation data is indeed as if it was taken randomly out of a traceless GUE. fig. 3.14 shows a plot of the combined eigenvalue distribution for the simulation and for the distribution in eq. (3.17) with α from table 3.1 (for $N = 9$). The distributions match almost exactly.

Next, we compare the distributions of $\mathrm{Tr}\left(X^1\right)^2$ and $\mathrm{Tr}\, X^i X^i$. In these cases, we know the analytical form of the distributions (gamma distributions). figs. 3.15 and 3.16 show the comparison. One observes that as we sum more of the $\mathrm{Tr}\, X^i X^i$, there is a significant departure from random matrix behavior. Limited evidence suggests that this is a finite N phenomenon, and as one approaches larger N, these deviations disappear, but more work needs to be done to verify these claims. In particular, we need to access larger values of N.

3.5 Departure from random matrix behavior

Interestingly, the deviation from traceless GUE for $\mathrm{Tr}\, X^i X^i$ cannot be attributed to sampling error or looking at an odd observable alone. This is because the time statistics of relatively high order of $\mathrm{Tr}\, X^i X^i$ still show universal, initial condition-independent behavior. However, these higher-order solution-independent statistics differ significantly from their tGUE counterparts.

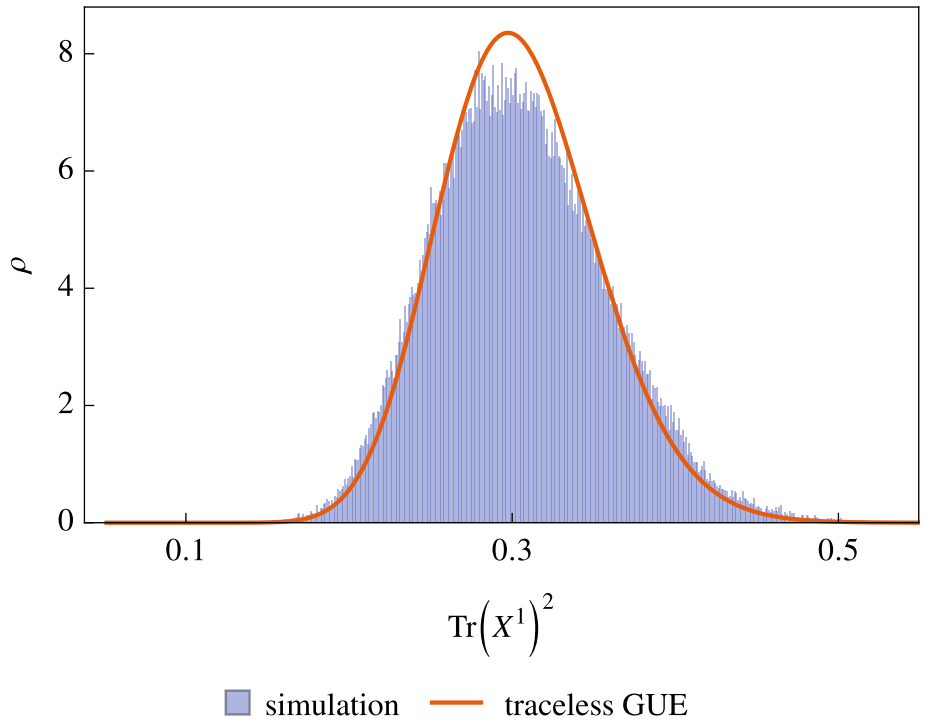

Figure 3.15: distribution of $\mathrm{Tr}\left(X^1\right)^2$ compared for the simulation data and the distribution from eq. (3.17) (a gamma distribution) with the same parameters as in fig. 3.14.

Let us quickly define the statistics we look at. For simplicity, let us denote the n^{th} central moment by c_n. Mean (c_1) and variance (c_2) are as usual, but we look at two new statistics

a. **Skewness** (b_1): This is related to the third central moment c_3 as

$$b_1 = \frac{c_3}{(c_2)^{3/2}} \tag{3.31}$$

b. **Kurtosis** (b_2): Related to the fourth central moment c_4

$$b_2 = \frac{c_4}{(c_2)^2} \tag{3.32}$$

table 3.2 summarizes these statistics for three sets of simulation data starting at random initial conditions and lastly for traceless GUE (eq. (3.17)) with α from table 3.1. Note that even higher order statistics like b_1 and b_2 are consistent across multiple initial conditions but depart significantly from traceless GUE.

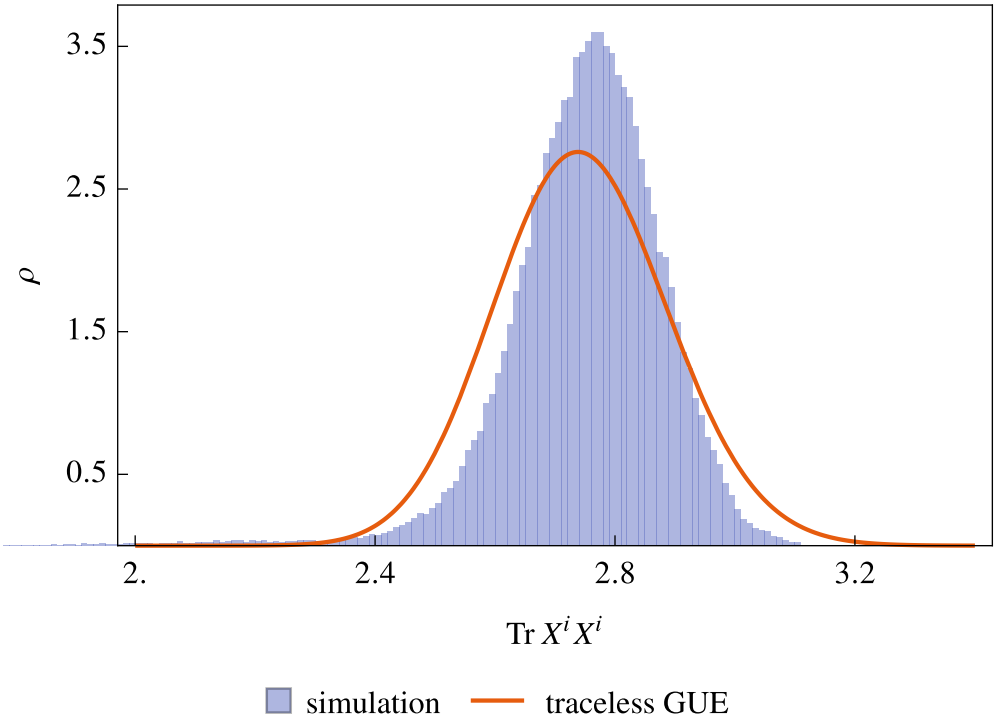

Figure 3.16: Distribution of Tr $X^i X^i$. Note how even though the means agree, the higher moments differ quite a bit (e.g., the simulation data is much more skewed than the gamma distribution).

Type	**Mean**	**Standard Deviation**	**Skewness**	**Kurtosis**
Random 1	2.742	0.1367	-1.62	15.89
Random 2	2.746	0.1376	-1.733	15.86
Random 3	2.74	0.1417	-1.59	14.23
Traceless GUE	2.746	0.1446	0.1208	3.067

Table 3.2: Higher order statistics for Tr $X^i X^i$ at $N = 9$ for random states and traceless GUE

These could be indications of significant higher-order correlations between the matrix variables that are not taken into account by the simple form of eq. (3.17). More work is needed to show that these correlations become unimportant at larger N.

CHAPTER

FOUR

DISCUSSION

In this thesis, we have presented original results on the classical real-time simulations of the bosonic sector of the BFSS matrix model. The results presented can be briefly summarized as follows

a. The matrix model is highly chaotic. This is not a new result (see [39, 40]), but what we observe is something really interesting: the nature of sensitivity to initial conditions in this model is such that states very close to each other get farther and farther as time evolves until a certain time t_S when the distance saturates and remains stable for all future times.

b. Long-time statistics of many low-order observables such as $\mathrm{Tr}\, X^i X^i$ and the eigenvalues of the matrices are by-and-large independent of the initial condition one starts at, as long as we work in a constant energy surface. The dependence of various statistics on the energy of the state follows very simply from scaling arguments of eq. (2.8).

c. By looking at the statistics of these observables, one finds an interesting connection to random matrices: the time distribution of the matrix variables look as if they were taken identically and independently from a traceless Gaussian Unitary Ensemble with a scale parameter α that depends only on the rank N of the gauge group and the energy E (in a simple manner due to scaling) of the state. At fixed energy, the scale parameter almost goes like $\alpha_N \sim \sqrt{N}$.

Random matrix theory has been very successful at describing late-time horizon dynamics of certain black holes [41]. The fact that we find random matrix behavior in the matrix model and the typicality of states suggests that classical time-dependent coherent states in matrix theory somehow mimic individual microstates of the dual black hole.

4.1 Future plans

In the future, we plan to investigate if including the fermionic matrices θ changes the picture we see. The states we study break all of the supersymmetry the original BFSS model has (16 supercharges). Could time-dependent states that preserve some of the supersymmetry offer new results not captured by the bosonic model we have been studying?

Secondly, we plan to include quantum corrections to the classical picture outlined in the thesis. To do this, we plan to use generalized coherent states highly localized on the classical solutions we have studied and look at how quantum mechanical corrections change the time evolution of such states and their spread in the space of solutions. This will allow us to make contact with energy regimes in which some semiclassical supergravity results might still be valid.

The results outlined in this dissertation are a small step towards a broader understanding of the emergence of space-time from quantum mechanical matrix models. Interpretations simplify at large N, but an interesting open question is what to make of the effective geometry at finite N. Is it a non-commutative dynamical space-time? Much remains to be explored.

REFERENCES

[1] Joseph Polchinski. "M theory and the light cone". In: *Prog. Theor. Phys. Suppl.* 134 (1999). Ed. by S. Iso, H. Kawai, and M. Natsuume, pp. 158–170. DOI: 10.1143/PTPS.134.158. arXiv: hep-th/9903165.

[2] Leonard Susskind. "The World as a hologram". In: *J. Math. Phys.* 36 (1995), pp. 6377–6396. DOI: 10.1063/1.531249. arXiv: hep-th/9409089.

[3] Juan Martin Maldacena. "The Large N limit of superconformal field theories and supergravity". In: *Adv. Theor. Math. Phys.* 2 (1998), pp. 231–252. DOI: 10.1023/A:1026654312961. arXiv: hep-th/9711200.

[4] Ofer Aharony et al. "Large N field theories, string theory and gravity". In: *Phys. Rept.* 323 (2000), pp. 183–386. DOI: 10.1016/S0370-1573(99)00083-6. arXiv: hep-th/9905111.

[5] Edward Witten. "Anti-de Sitter space and holography". In: *Adv. Theor. Math. Phys.* 2 (1998), pp. 253–291. DOI: 10.4310/ATMP.1998.v2.n2.a2. arXiv: hep-th/9802150.

[6] Lorenz Eberhardt, Matthias R. Gaberdiel, and Rajesh Gopakumar. "Deriving the AdS_3/CFT_2 correspondence". In: *JHEP* 02 (2020), p. 136. DOI: 10.1007/JHEP02(2020)136. arXiv: 1911.00378 [hep-th].

[7] Matthias R. Gaberdiel and Rajesh Gopakumar. "String Dual to Free N=4 Supersymmetric Yang-Mills Theory". In: *Phys. Rev. Lett.* 127.13 (2021), p. 131601. DOI: 10.1103/PhysRevLett.127.131601. arXiv: 2104.08263 [hep-th].

[8] Jorge Casalderrey-Solana et al. *Gauge/String Duality, Hot QCD and Heavy Ion Collisions*. Cambridge University Press, 2014. ISBN: 978-1-139-13674-7. DOI: 10.1017/CBO9781139136747. arXiv: 1101.0618 [hep-th].

[9] Youngman Kim, Ik Jae Shin, and Takuya Tsukioka. "Holographic QCD: Past, Present, and Future". In: *Prog. Part. Nucl. Phys.* 68 (2013), pp. 55–112. DOI: 10.1016/j.ppnp.2012.09.002. arXiv: 1205.4852 [hep-ph].

[10] Subir Sachdev. "Condensed Matter and AdS/CFT". In: *Lect. Notes Phys.* 828 (2011), pp. 273–311. DOI: 10.1007/978-3-642-04864-7_9. arXiv: 1002.2947 [hep-th].

[11] Kristan Jensen. "Chiral anomalies and AdS/CMT in two dimensions". In: *JHEP* 01 (2011), p. 109. DOI: 10.1007/JHEP01(2011)109. arXiv: 1012.4831 [hep-th].

[12] Ahmed Almheiri et al. “The Page curve of Hawking radiation from semiclassical geometry”. In: *Journal of High Energy Physics* 2020.3 (Mar. 2020). ISSN: 1029-8479. DOI: 10.1007/jhep03(2020)149. URL: http://dx.doi.org/10.1007/JHEP03(2020)149.

[13] Fridhrik Freyr Gautason et al. “Page Curve for an Evaporating Black Hole”. In: *JHEP* 05 (2020), p. 091. DOI: 10.1007/JHEP05(2020)091. arXiv: 2004.00598 [hep-th].

[14] Mariano Cadoni and Andrea Pierfrancesco Sanna. “Unitarity and Page Curve for Evaporation of 2D AdS Black Holes”. In: (June 2021). DOI: 10.3390/e24010101. arXiv: 2106.14738 [hep-th].

[15] Pinaki Banerjee. *Some basics of AdS/CFT*. https://www.imsc.res.in/~pinakib/AdS-CFT_ST4.pdf. [Online]. 2017.

[16] Tom Banks et al. “M theory as a matrix model: A Conjecture”. In: *Phys. Rev. D* 55 (1997), pp. 5112–5128. DOI: 10.1103/PhysRevD.55.5112. arXiv: hep-th/9610043.

[17] E. Cremmer, B. Julia, and Joel Scherk. “Supergravity Theory in Eleven-Dimensions”. In: *Phys. Lett. B* 76 (1978), pp. 409–412. DOI: 10.1016/0370-2693(78)90894-8.

[18] Juan Maldacena and Alexey Milekhin. “To gauge or not to gauge?” In: *JHEP* 04 (2018), p. 084. DOI: 10.1007/JHEP04(2018)084. arXiv: 1802.00428 [hep-th].

[19] Leonard Susskind. “Some speculations about black hole entropy in string theory”. In: (Oct. 1993). Ed. by C. Teitelboim and J. Zanelli, pp. 118–131. arXiv: hep-th/9309145.

[20] Gary T. Horowitz and Joseph Polchinski. “A Correspondence principle for black holes and strings”. In: *Phys. Rev. D* 55 (1997), pp. 6189–6197. DOI: 10.1103/PhysRevD.55.6189. arXiv: hep-th/9612146.

[21] Samir D. Mathur. “The Fuzzball proposal for black holes: An Elementary review”. In: *Fortsch. Phys.* 53 (2005). Ed. by E. Kiritsis, pp. 793–827. DOI: 10.1002/prop.200410203. arXiv: hep-th/0502050.

[22] Suvrat Raju and Pushkal Shrivastava. “Critique of the fuzzball program”. In: *Phys. Rev. D* 99.6 (2019), p. 066009. DOI: 10.1103/PhysRevD.99.066009. arXiv: 1804.10616 [hep-th].

[23] Washington Taylor. “M(atrix) Theory: Matrix Quantum Mechanics as a Fundamental Theory”. In: *Rev. Mod. Phys.* 73 (2001), pp. 419–462. DOI: 10.1103/RevModPhys.73.419. arXiv: hep-th/0101126.

[24] Adel Bilal. “M(atrix) theory : A Pedagogical introduction”. In: *Fortsch. Phys.* 47 (1999). Ed. by J. P. Derendinger and C. Lucchesi, pp. 5–28. DOI: 10.1002/(SICI)1521-3978(199901)47:1/3<5::AID-PROP5>3.0.CO;2-B. arXiv: hep-th/9710136.

[25] Badis Ydri. “Review of M(atrix)-Theory, Type IIB Matrix Model and Matrix String Theory”. In: (Aug. 2017). arXiv: 1708.00734 [hep-th].

[26] Nissan Itzhaki et al. “Supergravity and the large N limit of theories with sixteen supercharges”. In: *Phys. Rev. D* 58 (1998), p. 046004. DOI: 10.1103/PhysRevD.58.046004. arXiv: hep-th/9802042.

[27] Mark Claudson and Martin B. Halpern. “Supersymmetric Ground State Wave Functions”. In: *Nucl. Phys. B* 250 (1985), pp. 689–715. DOI: 10.1016/0550-3213(85)90500-0.

[28] B. de Wit, J. Hoppe, and H. Nicolai. “On the Quantum Mechanics of Supermembranes”. In: *Nucl. Phys. B* 305 (1988), p. 545. DOI: 10.1016/0550-3213(88)90116-2.

[29] Joseph Polchinski. “Tasi lectures on D-branes”. In: *Theoretical Advanced Study Institute in Elementary Particle Physics (TASI 96): Fields, Strings, and Duality*. Nov. 1996, pp. 293–356. arXiv: hep-th/9611050.

[30] Michael R. Douglas et al. “D-branes and short distances in string theory”. In: *Nucl. Phys. B* 485 (1997), pp. 85–127. DOI: 10.1016/S0550-3213(96)00619-0. arXiv: hep-th/9608024.

[31] Sonia Paban, Savdeep Sethi, and Mark Stern. “Constraints from extended supersymmetry in quantum mechanics”. In: *Nucl. Phys. B* 534 (1998), pp. 137–154. DOI: 10.1016/S0550-3213(98)00518-5. arXiv: hep-th/9805018.

[32] Daniel N. Kabat and Washington Taylor. “Linearized supergravity from matrix theory”. In: *Phys. Lett. B* 426 (1998), pp. 297–305. DOI: 10.1016/S0370-2693(98)00281-0. arXiv: hep-th/9712185.

[33] Masanori Hanada. “Monte Carlo approach to the string/M-theory”. In: *PoS* LATTICE2012 (2012). Ed. by Derek Leinweber et al., p. 019. DOI: 10.22323/1.164.0019. arXiv: 1212.2814 [hep-lat].

[34] Konstantinos N. Anagnostopoulos et al. “Monte Carlo studies of supersymmetric matrix quantum mechanics with sixteen supercharges at finite temperature”. In: *Phys. Rev. Lett.* 100 (2008), p. 021601. DOI: 10.1103/PhysRevLett.100.021601. arXiv: 0707.4454 [hep-th].

[35] Masanori Hanada et al. “Higher derivative corrections to black hole thermodynamics from supersymmetric matrix quantum mechanics”. In: *Phys. Rev. Lett.* 102 (2009), p. 191602. DOI: 10.1103/PhysRevLett.102.191602. arXiv: 0811.3102 [hep-th].

[36] Edward Witten. “Anti-de Sitter space, thermal phase transition, and confinement in gauge theories”. In: *Adv. Theor. Math. Phys.* 2 (1998). Ed. by L. Bergstrom and U. Lindstrom, pp. 505–532. DOI: 10.4310/ATMP.1998.v2.n3.a3. arXiv: hep-th/9803131.

[37] Georg Bergner et al. “Confinement/deconfinement transition in the D0-brane matrix model – A signature of M-theory?” In: *JHEP* 05 (2022), p. 096. DOI: 10.1007/JHEP05(2022)096. arXiv: 2110.01312 [hep-th].

[38] Abhishek Chowdhury et al. “Do All BPS Black Hole Microstates Carry Zero Angular Momentum?” In: *JHEP* 04 (2016), p. 082. DOI: 10.1007/JHEP04(2016)082. arXiv: 1511.06978 [hep-th].

[39] Evan Berkowitz, Masanori Hanada, and Jonathan Maltz. "Chaos in Matrix Models and Black Hole Evaporation". In: *Phys. Rev. D* 94.12 (2016), p. 126009. DOI: 10.1103/PhysRevD.94.126009. arXiv: 1602.01473 [hep-th].

[40] Guy Gur-Ari, Masanori Hanada, and Stephen H. Shenker. "Chaos in Classical D0-Brane Mechanics". In: *JHEP* 02 (2016), p. 091. DOI: 10.1007/JHEP02(2016)091. arXiv: 1512.00019 [hep-th].

[41] Jordan S. Cotler et al. "Black Holes and Random Matrices". In: *JHEP* 05 (2017). [Erratum: JHEP 09, 002 (2018)], p. 118. DOI: 10.1007/JHEP05(2017)118. arXiv: 1611.04650 [hep-th].

[42] Robert I. McLachlan. "On the Numerical Integration of Ordinary Differential Equations by Symmetric Composition Methods". In: *SIAM Journal on Scientific Computing* 16.1 (1995), pp. 151–168. DOI: 10.1137/0916010. eprint: https://doi.org/10.1137/0916010. URL: https://doi.org/10.1137/0916010.

[43] B. Schäling. *The Boost C++ Libraries*. Boris Schäling. URL: https://books.google.fr/books?id=2jUVBQAAQBAJ.

[44] Craig A. Tracy and Harold Widom. "On the Distributions of the Lengths of the Longest Monotone Subsequences in Random Words". In: *arXiv Mathematics e-prints*, math/9904042 (Apr. 1999), math/9904042. DOI: 10.48550/arXiv.math/9904042. arXiv: math/9904042 [math.CO].

[45] Giacomo Livan, Marcel Novaes, and Pierpaolo Vivo. *Introduction to Random Matrices*. Springer International Publishing, 2018. DOI: 10.1007/978-3-319-70885-0. URL: https://doi.org/10.1007%2F978-3-319-70885-0.

APPENDICES

APPENDIX

A

NUMERICAL METHODS

The initial data of the BFSS system are 9 $N \times N$ Hermitian matrices $X^1(0), \ldots, X^K(0)$ and their velocities $\dot{X}^1(0), \ldots, \dot{X}^K(0)$. Generating a random $N \times N$ Hermitian matrix is easy; generate N^2 random complex numbers using something like `RandomComplex` in Mathematica and assemble them into a complex $N \times N$ matrix Z and take the Hermitian part $\frac{1}{2}(Z + Z^\dagger)$.

The trace of the various matrices is unimportant because of "translation" symmetry $X^k \to X^k + \epsilon^k \mathbf{1}_N$ generated by the total momentum $\mathrm{Tr}\, \dot{X}^k$ which we set equal to zero, along with the center of mass position $\mathrm{Tr}\, X^k$, effectively working in the "center of mass" frame. We can thus remove traces of the various matrices above by $Z \to Z - \frac{\mathrm{Tr}\, Z}{N} \mathbf{1}_N$.

Of course, the problem with generating initial states like this is that they will generically be on completely disjoint phase trajectories. In order to study thermalization or some universal behavior, it is necessary to start with states of fixed macroscopic charges, which arise from the following symmetries.

1. **Time translation** $\quad t \to t + \epsilon \quad \delta X^k = -\epsilon \dot{X}^k$

$$E = \mathrm{Tr}\left(\frac{1}{2}\dot{X}^k \dot{X}^k - \frac{1}{4}\left[X^i, X^j\right]\left[X^i, X^j\right]\right) \tag{A.1}$$

2. $\mathrm{SO}(K)$ **Rotations** $\quad \omega_{kj} = -\omega_{jk} \quad \delta X^k = \omega_{kj} X^j$

$$J^{ij} = \mathrm{Tr}\left(X^i \dot{X}^j - X^j \dot{X}^i\right) \tag{A.2}$$

3. $\mathrm{SU}(N)$ **Gauge transformations** $\quad M^\dagger = -M \quad \delta X^k = \left[M, X^k\right]$

$$G = \left[X^k, \dot{X}^k\right] \tag{A.3}$$

To study the gauged system, G must be set to zero.

In total, there are $1 + \frac{K(K-1)}{2} + (N^2-1) + K = N^2 + \frac{K(K+1)}{2}$ real charges[1].

The simplest way to fix the charges and satisfy the Gauge constraint is to set all the initial velocities to zero

$$\dot{X}^i(0) = 0 \tag{A.4}$$

and we do exactly this.

It is very useful to rewrite the matrix variables in a convenient basis of the lie algebra $\mathfrak{su}(N)$ of $N \times N$ traceless Hermitian matrices. We use a generalized Gell-Mann type basis given by $\frac{N(N-1)}{2}$ real symmetric matrices, $\frac{N(N-1)}{2}$ imaginary antisymmetric matrices and $N-1$ real diagonal matrices (which also generate the Cartan subalgebra in this basis).

$$\underbrace{\frac{1}{2}\begin{pmatrix} & 1 & \\ 1 & & \\ & & \end{pmatrix}}_{\text{real symmetric}} \qquad \underbrace{\frac{1}{2}\begin{pmatrix} & -i & \\ i & & \\ & & \end{pmatrix}}_{\text{imaginary antisymmetric}}$$

$$\underbrace{\frac{1}{\sqrt{2r(r-1)}}\begin{pmatrix} 1 & & & \\ & \ddots & & \\ & & 1 & \\ & & & 1-r \end{pmatrix}}_{\text{real diagonal}} \tag{A.5}$$

These are normalized so that

$$\operatorname{Tr} t^a t^b = \frac{1}{2}\delta^{ab} \tag{A.6}$$

We chose the physicist's convention for the Lie algebra of $\mathrm{SU}(N)$, meaning that the fundamental commutation relations of the t^as contain a factor of i. They are

$$\left[t^a, t^b\right] = i f^{abc} t^c \tag{A.7}$$

It is easy to compute the structure constants f^{abc} in the basis we use eq. (A.5). Due to the diagonal Cartan-Killing form eq. (A.6), the structure constants are completely antisymmetric in this basis. We can now expand all our matrix degrees of freedom in this basis

$$X^i(t) = x^i_a(t) t^a \tag{A.8}$$

the matrix model equations of motion eq. (2.4) can then be written as

$$\ddot{x}^i_a = f^{aed} f^{ebc} x^i_b x^j_c x^j_d \tag{A.9}$$

As stated in Chapter 3, the initial "positions" $x^i_a(0)$ are taken to be random. In particular, the procedure we follow to generate them is

a. Generate $\tilde{X}^i_a$ as $K(N^2-1)$ random real numbers uniformly distributed in $(-1, 1)$.

[1]The last term is the translation symmetry charge, the total momentum, which we set to zero

b. Compute the energy E of this state (with no velocity contribution) as

$$E = \frac{1}{8} f^{abe} f^{cde} \tilde{X}^i_a \tilde{X}^j_b \tilde{X}^i_c \tilde{X}^j_d \tag{A.10}$$

c. The random initial state we study X^i_a is then given by

$$X^i_a = \lambda \tilde{X}^i_a \qquad \lambda = E^{-1/4} \tag{A.11}$$

By construction, the state just generated has energy $E = 1$. We now pose this as an initial value problem (IVP)

$$\dot{x}^i_a = p^i_a \qquad x^i_a(0) = X^i_a \tag{A.12}$$

$$\dot{p}^i_a = f^{aed} f^{ebc} x^i_b x^j_c x^j_d \qquad p^i_a(0) = 0 \tag{A.13}$$

Initial value problems (IVPs) are abundant in all of the sciences. There are numerous numerical methods and packages that can be used to solve IVPs of different types. The type of system we have, is, of course, a symplectic IVP since it is a Hamiltonian system. A standard numerical algorithm for solving symplectic systems is the Runge-Kutta-Nystroem family. We use the symplectic McLachlan symmetric B3A stepper implementing sixth order RKN [42].

As a platform for our simulations, we chose to write C++ programs to optimize computational resources as much as possible. The Boost C++ library [43] comes very handy in this regard as it already contains a robust implementation of symplectic RKN methods. Our simulation was run on the IITM Quantum cluster with parallel programming optimizations. An example of runtimes involved is: at $N = 9, K = 9$, and for a length of time $T = 1000$ and step size $dt = 0.1$, it takes around 5 hours on an Intel(R) Xeon(R) Gold 5220R CPU @ 2.20GHz on a single core.

APPENDIX

B

GAUSSIAN UNITARY ENSEMBLE

Perhaps the simplest distribution for an $N \times N$ complex matrix Y is one in which the real and imaginary parts of every matrix entry are distributed (independently and identically) according to a normal distribution. In particular, if

$$Y = (y_{ij})_{i,j=1}^{N} \tag{B.1}$$

then the distribution would be

$$\begin{aligned} p(y_{ij}) &= \prod_{ij} \frac{1}{2\pi\sigma^2} \exp\left(-\frac{1}{2\sigma^2} y_{ij}\overline{y}_{ij}\right) \\ &= \left(\frac{1}{2\pi\sigma^2}\right)^{N^2} \exp\left(-\frac{1}{2\sigma^2} \sum_{ij} y_{ij}\overline{y}_{ij}\right) \\ &= \frac{1}{Z} \exp\left(-\frac{1}{2\sigma^2} \operatorname{Tr} Y^{\dagger}Y\right) \end{aligned} \tag{B.2}$$

with

$$\log Z = N^2 \log\left(2\pi\sigma^2\right) \tag{B.3}$$

being the partition function used for normalization.

However, we are interested in traceless Hermitian matrices. But once one can generate random "normal" complex matrices Y, it is elementary to transform them into traceless Hermitian matrices. We do this in two steps

a. Pick out the Hermitian part $\tilde{X}$

$$Y \to \tilde{X} = \frac{Y + Y^{\dagger}}{2} \tag{B.4}$$

b. Remove the trace

$$\tilde{X} \to X = \tilde{X} - \frac{Tr\tilde{X}}{N}\mathbf{1}_N \tag{B.5}$$

The distribution of the random matrix variable $\tilde{X}$ has a distribution closely related to eq. (B.2), namely

$$p(\tilde{X}) = \frac{1}{Z_{\text{GUE}}} \exp\left(-\frac{1}{2\sigma^2} \operatorname{Tr} \tilde{X}^2\right) \tag{B.6}$$

This is called the Gaussian Unitary Ensemble (GUE). Although the functional form of the distribution looks very much like eq. (B.2), the partition function Z_{GUE} has changed since the probability measure now contains only half as many integration variables as before (N^2 now, $2N^2$ for Y).

Finally, removing the trace results in the so-called traceless GUE with, again, the same functional form for the distribution but a different partition function we call Z_{tGUE}.

It is interesting to look at the distribution of eigenvalues $(\lambda_1, \ldots, \lambda_N)$ resulting from, say, GUE. The joint distribution (for the case $\sigma = 1$) turns out to be

$$\rho(\lambda_1, \ldots, \lambda_N) = \frac{1}{\mathcal{Z}} e^{-\frac{1}{2}\sum_{i=1}^{N} \lambda_i^2} \prod_{i<j} (\lambda_i - \lambda_j)^2 \tag{B.7}$$

where $\mathcal{Z}$ is given by a kind of Mehta's integral

$$\mathcal{Z} = (2\pi)^{N/2} \prod_{k=1}^{N} k! \tag{B.8}$$

One can integrate out all but one of the eigenvalues to obtain the marginal distribution of one of the eigenvalues. It can be shown that it is the same distribution as what one would obtain if one were to combine all the eigenvalues and treat them independently (even though they are not independent). Incidentally, the non-independence of the eigenvalues results in physical phenomena where a random matrix description works, such as level repulsion. After a little bit of work and using the machinery of orthogonal polynomials, this results in

$$\rho_{\text{GUE}}(\lambda) = \frac{1}{N\sqrt{2\pi}} e^{-\lambda^2/2} \sum_{k=0}^{N-1} \frac{1}{2^k k!} H_k\left(\frac{\lambda}{\sqrt{2}}\right)^2 \tag{B.9}$$

where H_k denotes the k^{th} Hermite polynomial. Further, the asymptotic formulae for the Hermite polynomials can be used to prove the Wigner semicircle law (that holds as $N \to \infty$).

The corresponding formulae for traceless GUE can also be obtained with some work, but as of now, we do not have a closed-form distribution of eigenvalues. It is, however, interesting to note a relationship between the eigenvalue distribution of GUE and traceless GUE (see, e.g., [44]) that schematically looks like

$$\rho_{\text{GUE}}(\lambda) = \sqrt{\frac{N}{\pi}} \int_{\mathbb{R}} \mathrm{d}t\, e^{-Nt^2} \rho_{\text{tGUE}}(\lambda - t) \tag{B.10}$$

For an accessible introduction to the theory of random matrices, see [45].

APPENDIX

C

MATRIX SPHERICAL HARMONICS

In trying to understand a theory of matrices, it is useful to think of a configuration of them (traceless, Hermitian, in our case) as functions on S^2. In particular, these functions can be restricted to square integrable $L^2(S^2)$. Another way to approach this is by considering the matrices as a truncation of the set of all square-integrable functions on S^2. Thus, one has a map μ.

$$\begin{aligned} \mu \colon \mathfrak{u}(N) &\to L^2(S^2) \\ X &\mapsto \mu(X) \end{aligned} \tag{C.1}$$

This map must respect the Hilbert space structure on the two sides. In addition, the two sides have a natural action of SU(2) defined on them. We can require our map to be equivariant with respect to this action. In total, we can list three requirements for μ

1. Linearity
$$\mu(\alpha X + \beta Y) \;=\; \alpha\,\mu(X) + \beta\,\mu(Y) \tag{C.2}$$

2. Preserve inner product
$$\underbrace{\frac{1}{N}\operatorname{Tr} X^\dagger Y}_{\substack{\text{Hilbert-Schmidt inner} \\ \text{product on } \mathfrak{u}(N)}} \;=\; \underbrace{\int_{S^2} \mathrm{d}\Omega\, \mu(X)^* \mu(Y)}_{L^2 \text{ inner product}} \tag{C.3}$$

3. Preserve the action of SU(2)
SU(2) acts on $\mathfrak{u}(N)$ by it's adjoint action. On S^2, SU(2) acts by rotation which is pushed over to $L^2(S^2)$
$$\begin{aligned} \mathfrak{u}(N) \ni X &\xrightarrow{U \in \mathrm{SU}(2)} U^\dagger X U \\ L^2(S^2) \ni f(\theta,\phi) &\xrightarrow{U \in \mathrm{SU}(2)} f(U^{-1}(\theta,\phi)) \\ U^\dagger X U &\xrightarrow{\mu} \mu(X)(U^{-1}(\theta,\phi)) \end{aligned} \tag{C.4}$$

Or, at the level of SU(2) generators $\mathfrak{g} = \alpha_i J^i$

$$\left[J^i, X\right] \xrightarrow{\mu} \xi^{(i)}(\mu(X)) \tag{C.5}$$

where $\xi^{(i)}$ are the Killing fields associated to J^i. Explicitly,

$$\xi^{(i)} = -i\epsilon_{ijk}x^j \frac{\partial}{\partial x^k} \quad \text{with} \quad x^k = (\sin\theta\cos\phi, \sin\theta\sin\phi, \cos\theta) \tag{C.6}$$

To explicitly construct such a map, it is enough to define it on a basis $\{\boldsymbol{Z}_a\}$ of $\mathfrak{u}(N)$. However, we would also like to make use of the rotational covariance, which is more manifest on the right-hand side of this map: We know that spherical harmonics Y^j_m ($j = 0, 1, \ldots$ and $m = -j, -j+1, \ldots, j$) give a convenient orthonormal basis of $L^2(\boldsymbol{S}^2)$ which also transforms nicely under $\mathfrak{su}(2)$. That is, every j-multiplet of Y^j_m furnishes the usual spin-j representation of $\mathfrak{su}(2)$. For example,

$$\begin{aligned} \xi^3 Y^j_m &= m Y^j_m \\ \xi^i \xi^i Y^j_m &= j(j+1) Y^j_m \\ \frac{1}{4\pi}\int_{S^2} \mathrm{d}\Omega\, {Y^{j_1}_{m_1}}^* Y^{j_2}_{m_2} &= \delta^{j_1}_{j_2}\delta^{m_1}_{m_2} \end{aligned} \tag{C.7}$$

Thus, if we can define the inverse map μ^{-1} on these Y^j_m, we'd be done. It is clear, though, that the map μ as it is defined above fails to be surjective: $L^2(\boldsymbol{S}^2)$ is an infinite dimensional vector space whereas $\mathfrak{u}(N)$ is N^2 dimensional. However, we can still define μ on a truncated set of Y^j_m. The truncation is easy to derive: each j-multiplet is $(2j+1)$ dimensional. Suppose we truncate at $j = j_{\max}$: i.e., we only take $j \in \{0, 1, \ldots, j_{\max}\}$, then it must be that

$$\sum_{j=0}^{j_{\max}} (2j+1) = (j_{\max}+1)^2 = N^2 \qquad \Longrightarrow \qquad j_{\max} = N-1 \tag{C.8}$$

Therefore, we must define the so-called *matrix harmonics* $Z^j_m \coloneqq \mu^{-1}(Y^j_m)$ ($j = 0, 1, \ldots, N-1$ and $m = -j, -j+1, \ldots, j$)

Fortunately, we do have some special $\mathfrak{u}(N)$ matrices that can help: the spin-$\frac{N-1}{2}$ dimensional representation of $\mathfrak{su}(2)$. For the spin-j irrep

$$J^3_{ss'} \coloneqq \langle j\, s' | J^3 | j\, s\rangle = s\, \delta_{ss'} \tag{C.9}$$

And J^1, J^2 are given in terms of $J^\pm \coloneqq J^1 \pm iJ^2$

$$\begin{aligned} J^\pm_{ss'} &= C^\pm_{js}\, \delta_{s\pm1,s'} \\ C^\pm_{js} &= \sqrt{(j \mp s)(j \pm s + 1)} \end{aligned} \tag{C.10}$$

The Z^j_m can be found by starting at the lowest "rung of the ladder," Z^j_{-j} and successively applying J^+

$$Z^j_m = \frac{1}{C^+_{j\,m-1}}\left[J^+, Z^j_{m-1}\right] \tag{C.11}$$

Note that $\left[J^-, Z^j_{-j}\right] = 0$ so a plausible choice could be $Z^j_{-j} = f(J^-)$. Also, $[J^+, (J^-)^m] \sim (J^-)^{m-1}$, so we take

$$Z^j_{-j} = c\,(J^-)^j \tag{C.12}$$

where c is found by requiring orthonormality

$$\frac{1}{N}\,\mathrm{Tr}\left(Z^{j_1}_{m_1}\right)^\dagger Z^{j_2}_{m_2} = \delta^{j_1}_{j_2}\delta^{m_1}_{m_2} \tag{C.13}$$